The lithium isotope response to the variable weathering of soils in Iceland

Philip A.E. Pogge von Strandmann[1,2*], Kevin W. Burton[3], Sophie Opfergelt[4], Bianca Genson[2], Rannveig A. Guicharnaud[5], Sigurður R. Gislason[6]

[1]Institute of Geosciences, Johannes Gutenberg University, 55122 Mainz, Germany.
[2]Institute of Earth and Planetary Sciences, University College London and Birkbeck, University of London, Gower Street, London, WC1E 6BT, UK.
[3]Department of Earth Sciences, Durham University, Durham, DH1 3LE, UK.
[4]Earth and Life Institute, Université catholique de Louvain, Croix du Sud 1 bte L7.05.10, 1348 Louvain-la-Neuve, Belgium.
[5]Icelandic Institute of Natural History, Urriðaholtsstræti 6-8, 210 Garðabær, Iceland.
[6]Institute of Earth Sciences, University of Iceland, Reykjavik, Iceland.

*Corresponding author: ppoggevo@uni-mainz.de

Abstract

This study has analysed Li isotopes ratios from well-studied soil and pore water profiles from Iceland that have the same parent material but have experienced different degrees of chemical weathering. Thus, from least to most weathered, we have analysed vitrosols (V), gleyic andosols (GA), brown andosols (BA), Histosols (H) and Histic Andosols (HA). Although the most weathered H and HA soils have the highest content in clay-sized material, they have the least fractionated $\delta^7Li_{pore\ water}$ values. In contrast, the least weathered GA and BA pore waters are most fractionated for Li isotopes. Given that Li isotope ratios are

fractionated by clay mineral formation, this appears counter-intuitive. A single trend for all samples of δ^7Li as a function of Li/Na ratios suggests that they are all controlled by a process with a single fractionation factor, in this case likely the formation of poorly-crystalline allophane, which dominates in the "least weathered" soils. This rapidly forming secondary mineral dominates Li isotope fractionation over more slowly-forming crystalline clays. The fractionation along a single path shows that the key process here in controlling the Li isotope ratio of surface waters is the degree of Li uptake by secondary minerals. This does not necessarily correspond to the amount of clay minerals present in the soil, but to the amount of clay minerals that are being newly formed in a single passage of the pore water through the soil, or are in equilibrium with soil solutions at the time of sampling.

1.0 Introduction

The chemical weathering of rocks at the Earth's surface is the primary control on atmospheric CO_2 levels on varying timescales. Weathering provides both alkalinity (stemming from water-rock-atmospheric-carbon interactions) and cations for the formation of marine carbonates, sequestering carbon (Berner et al., 1983; Walker et al., 1981). If the rocks being weathered are silicates, containing virtually no carbon, then this carbon sequestration is a net sink and a primary long-term climate controlling process. At the same time, continental weathering provides a number of critical nutrients (e.g. iron, silicon, phosphorus) to the coastal oceans, which stimulates primary productivity (Hawley et al., 2017; Lalonde et al., 2012). This productivity temporarily also takes up atmospheric carbon, but most marine organic matter is reoxidised before it is buried in marine sediments. However, continental chemical weathering and physical erosion also provide clay particles into the coastal oceans. These both increase nutrient fluxes to primary productivity (because microbes leach nutrients from the rock particles (Grimm et al., 2019)), but, critically, also greatly increase organic

carbon burial, thus also sequestering carbon on the long term (Kennedy et al., 2014; Kennedy and Wagner, 2011). Overall, this makes silicate weathering the primary atmospheric CO_2 controlling process on both long (via carbonate precipitation) and short, seasonal timescales (via organic carbon burial).

Significant effort has focused on understanding and quantifying weathering processes and fluxes, as well as on the processes that control weathering (Gislason et al., 2009; Maher, 2011; West et al., 2005). In particular, a feedback control, via a temperature-driven "thermostat" is likely to be the overarching process that has mitigated climate over geological time, although time periods also exist where an increase in supply may have overridden this climate stabilisation process, such as in the Cenozoic (Raymo and Ruddiman, 1992).

The debates on these various processes have been at the forefront of biogeochemistry for almost four decades, but finding reliable and unambiguous tracers of weathering processes both in the present and geological past has proven tricky. One of the most established of such tracers is lithium isotopes. Lithium is a moderately incompatible trace element that is present in all silicate rocks, in orders of magnitude more than in carbonate rocks (Penniston-Dorland et al., 2017; Pogge von Strandmann et al., 2020). Hence, in weathering environments, Li arises from the dissolution of silicates, even in carbonate-dominated catchments (Kisakürek et al., 2005; Millot et al., 2010). Lithium isotopes (^{6}Li and ^{7}Li) are not fractionated by primary productivity (Pogge von Strandmann et al., 2016), and while it remains poorly understood whether plants fractionate Li isotopes, the Li concentration of plants is sufficiently low for surface waters to remain largely unaffected (Clergue et al., 2015; Lemarchand et al., 2010; Li et al., 2020; Steinhoefel et al., 2021). Instead, Li isotopes are fractionated by the silicate weathering process, in that when primary silicate rocks (with a relatively low isotope ratio) are dissolved, they impart a low (rock-like) δ^7Li to waters. Isotopically light lithium is preferentially taken up by formation of secondary

minerals (clays, oxides, zeolites), as well as by adsorption onto secondary minerals, imparting a heavy isotopic signature to residual waters (Chan et al., 1992; Hindshaw et al., 2019; Huh et al., 2001; Millot et al., 2010; Pistiner and Henderson, 2003; Pogge von Strandmann et al., 2019a; Pogge von Strandmann et al., 2017b; Pogge von Strandmann and Henderson, 2015; Teng et al., 2010; Vigier et al., 2008). Consequently, dissolved Li isotopes are controlled by the weathering congruency: congruent dissolution of silicates imparts a low δ^7Li, while incongruent weathering (where secondary minerals form) yields a high δ^7Li signature relative to the parent material (Misra and Froelich, 2012; Pogge von Strandmann and Henderson, 2015).

Li isotopes are now well established as a tracer of both present and past weathering processes (Dellinger et al., 2015; Hathorne and James, 2006; Lechler et al., 2015; Misra and Froelich, 2012; Pogge von Strandmann et al., 2021a; Pogge von Strandmann et al., 2017a; Pogge von Strandmann et al., 2013), but important questions remain, especially concerning precisely how Li isotopes respond to changes in weathering processes. For example, the effect of water-rock interaction time (e.g. secondary mineral formation rates) on Li isotopes remains poorly quantified, partly because the timing of adsorption vs. incorporation during neoformation is poorly known, and because the effect of Li uptake by oxides/oxyhydroxides vs. clay or zeolites is also poorly known (Hindshaw et al., 2019; Li and Liu, 2020). This study aims to investigate the, as yet, little quantified effects arising from variable degrees of weathering in soils – for example, high solution δ^7Li could be due to either a high fraction of removal with a low fractionation factor, or lower removal with a high fractionation factor. Here we examine soil and pore water profiles from different soil types from Iceland. These different profiles represent weathering of bedrock with a similar composition, but reflect differing degrees of weathering.

2.0 Samples

Five different Icelandic soil types were analysed that represent increasing degrees of chemical weathering, collected in 2009 and 2010 (Opfergelt et al., 2014), and are shown on a soil map of Iceland (Fig. 1). These particular samples have previously been analysed for the isotopes of Mg, Si, Fe and Zn (Opfergelt et al., 2014; Opfergelt et al., 2017a; Opfergelt et al., 2017b). These Icelandic soils have specific definitions (Arnalds, 2004): Vitrisols (V) represent the least weathered soils from Iceland, and have <1% organic carbon or <1% Si_{ox}. Their mineralogy is dominated by volcanic glass, and they have little (5–10%) plant cover. Broadly, they represent a desert-like environment with little vegetation or soil formation, but in a cold and wet environment.

Gleyic andosols (GA – where US spelling is Andisols) are slightly more weathered, and tend to have organic carbon contents (<12%) in surface horizons. They contain allophane contents of up to 20%.

Brown andosols (BA) are increasingly weathered, and are the classical freely drained andosols found in Iceland. They tend to contain significant allophane (15–30%), as well as some ferrihydrite (1–8%).

Histosols (H) and Histic Andosols (HA) are the most weathered soils in this study. Histosols are dominated by organic materials (>20% organic C). Histic Andosols are found in poorly drained areas, and have sufficient aeolian inputs to reduce their organic contents below the 20% limit for Histosols. Allophane content is 2–10%, and they meet the $(Al + 0.5Fe)_{ox}$ criteria for Andosols.

Overall, Iceland is covered by ~48% Andosols (of all types), ~40% Vitrisols and Leptosols and ~1% Histosols (and 11% by glaciers and ice caps) (Arnalds, 2004). In general, vegetated areas are dominated by Andosols, desert areas by Vitrisols and wetlands by Histosols.

In this study, the vitrisol (V) is from SW Iceland, located south of the Langjökull and west of the Myrdalsjökull ice caps. The gleyic andosol (GA) is from just north of Reykjavik. The brown andosol (BA), the Histosol (H), and the Histic Andosol (HA) are from the Borgarfjörður catchment in western Iceland. Peats were developed at the HA and H sites (Opfergelt et al., 2014). Overall, GA and BA soils are well-drained, while the H and HA soils are poorly drained, with inevitable consequences for the water-rock interaction time. All soils developed from similar tholeiitic basalt, and their difference from each other is largely due to the soil drainage conditions (Opfergelt et al., 2014).

Further to the soils, a series of local secondary minerals was acquired from the Natural History Museum in Reykjavik. These minerals were not always formed in the same areas as the soils (although many are from the same catchment), but are from similar Icelandic weathering environments, and are examined here to provide some context of secondary mineralogy. These include samples of different calcites, clays (unidentified) and six different types of zeolite (heulandite, chabazite, mesolite, stilbite, epistilbite and scolecite). Further, an Fe-oxyhydroxide was taken from the coating on a pebble from a side stream on the nearby Norðura River (locality A6; (Pogge von Strandmann et al., 2006)). The major element composition suggests that this coating is largely impure ferrihydrite, containing Al, P and possibly Si admixtures (Si not measured), typical of soil and stream environments, but the presence of other phases, such as Al-hydroxide, cannot be ruled out.

3.0 Methods

3.1 Sampling

Sampling is described in Opfergelt et al. (2014). Briefly, typical parent tholeiitic basalt was sampled at the BA site. This represents the type of parent material for the HA, H, BA and GA sites. For the Vitrisol, the C horizon was considered as unweathered parent

151 volcanic ash. Soil profiles were described following FAO guidelines and sampled by horizon.
152 Soil samples were air-dried and sieved at 2mm. The measurement of chemical and physical
153 properties of the soils (pH, cation exchange capacity (CEC), chemical composition) is
154 described by Opfergelt et al. (2014).

155 Three representative soils were sequentially leached to separate out different phases,
156 and analysed for Li concentrations. The leaching technique followed a modified version of
157 Tessier et al. (1979) detailed in Revels et al. (2021). Briefly, the exchangeable fraction was
158 leached using $Mg(NO_3)_2$ at pH5 for 1 hour; carbonates were leached using acetic acid
159 buffered with Na acetate to pH5 for 5 hours; oxides were leached using NH_2OH-HCl in
160 acetic acid at 96°C; the silicate residue was dissolved using the method described for bulk
161 soils below.

162 Soil solutions were sampled over two different seasons (September 2009 and June
163 2010), using macro rhizon soil water samplers, which filter pore waters at 0.2 μm. Elemental
164 concentrations were determined by ICP-MS and ion chromatography, as described by
165 Opfergelt et al. (2014). In their initial measurements, Li concentrations were not always
166 determined, because [Li] was so low, and was hence below detection limits. For these
167 samples, Li concentration was re-determined by this study during isotope analysis, by drying
168 down at least 10ml of sample, and comparing the MC-ICP-MS beam intensity to that of a
169 known concentration standard.

170

171 *3.2 Li isotope analyses*

172 Lithium isotope purification and analyses by our methods have been described in
173 elsewhere (Pogge von Strandmann et al., 2011; Pogge von Strandmann and Henderson,
174 2015). Briefly, soils were dissolved in HF-HNO_3-$HClO_4$, HNO_3 and HCl, and sufficient pore
175 water was dried down to attain 20ng Li. This was purified through a two-step cation

exchange method, and analysed relative to the LSVEC standard on a Nu Instruments HR MC-ICP-MS at Oxford University. Splits taken before and after the Li collection bracket on the columns show that >99.9% of Li analysed, which is essential for both precision and accuracy. The total procedural blank for Li isotopes is effectively undetectable (<0.005 ng Li). Long-term precision of this method and instrument is ±0.6‰ (2sd), based on repeated seawater analyses of 31.2 ± 0.6‰ (2sd, n = 62), and BCR-2 basalt of 2.6 ± 0.4‰ (n = 6).

4.0 Results

Opfergelt et al. (2014) extensively characterised these soils, and results are given in Tables 1 and 2. Briefly, the primary mineralogy of these soils (augite, Ca-plagioclase, magnetite) reflects that of the primary tholeiitic basalt. Based on selective extraction, secondary minerals are dominated by short-range ordered minerals, mainly allophane and ferrihydrite, as also reported from other Icelandic soils (Arnalds, 2004; Sigfússon et al., 2006, 2008). No other secondary minerals were identified in the soils' clay-sized fraction (<2μm), except in the HA soil, where XRD detected smectite and kaolinite (Opfergelt et al., 2014). The allophane content is higher in the V-BA-GA soils than in the HA-H soils. This is because allophane forms above pH 4.9 when Al is not complexing with humus and therefore the more acidic HA-H soils have a lower allophane content (Mizota and van Reeuwiik, 1989). The HA-H soils do contain some allophane, which is explained by aeolian deposition or by higher pH conditions that may have existed earlier in the soil development cycle (Opfergelt et al., 2014).

As described by Opfergelt et al. (2014), one of the primary chemical properties of the bulk soils is the total reserve in bases (TRB = [Na] + [Mg] + [Ca] + [K]). The TRB is well-defined as a relative index quantifying the leaching of these cations in the soils relative to the parent material (e.g. Ameijeiras-Mariño et al., 2017; Delvaux et al., 1989; Henriet et al.,

2008), and hence provides an estimate of the content of the weatherable minerals in the soils. Any fraction of cations that are included in present secondary, rather than primary minerals, will still be included in the TRB. The TRB value in soils decreases with increased weathering, and leads to the observation that the least weathered soil is the Vitrisol (average TRB = 618 $cmol_c/kg$), compared to a value of 733 $cmol_c/kg$ in the pristine basalt, followed by the Gleyic Andosol (TRB = 401 $cmol_c/kg$), then the Brown Andosol (TRB = 358 $cmol_c/kg$), then the Histosol (TRB = 194 $cmol_c/kg$), closely followed by the Histic Andosol (TRB = 158 $cmol_c/kg$), which is therefore the most weathered soil type. This relative degree of weathering is supported by a direct correlation with the proportion of free Fe (Fe_d/Fe_t) (Opfergelt et al., 2017b), which is also used as a weathering indicator. This is also further supported by the total clay-sized content (<2μm), which is higher in the HA-H soils (53 and 43%, respectively) compared to the BA-GA (both ~35%) and V (4.6%) soils (Table 1).

4.1 Lithium in soils

None of the soil profiles have a clear trend in Li concentrations with depth (Fig. 2a). Overall, the GA soil has the highest Li concentrations (10.6 ± 2.8 (1sd) μg/g), followed by the BA and V (8.3 ± 2.6 and 8.3 ± 3.0 μg/g, respectively), and then by the H and HA (5.2 ± 3.3 and 5.2 ± 2.8 μg/g, respectively). In comparison, the host basalt has a Li concentration of 5.89 μg/g, within the range for Icelandic basalts (Pogge von Strandmann et al., 2006; Pogge von Strandmann et al., 2008; Pogge von Strandmann et al., 2012; Vigier et al., 2009).

The selective leaches of three soils (HA O1, H O6, BA BW2) show that between 0.2 and 3.4% of the total Li is in the exchangeable fraction, slightly less than observed during experiments with Icelandic basalts (Pogge von Strandmann et al., 2019a), but similar to the amount of Mg reported in this fraction (Opfergelt et al., 2014). Carbonates contain a similar proportion of Li (1–4%). The oxide fractions (primarily Fe-oxides) contain significantly more

Li, ranging from 10% in the BA soil, to 25% in the HA soil. The silicate fraction contains ~90% of the total Li in the BA soil, 70% in the HA soil, and 72% in the H soil (Table 1). Although the recovered phases are slightly different compared to the BCR leaching of Hawaiian basalt by Li et al. (2020) (e.g. that method combines exchangeable and carbonate phases in a single leach), the results agree in that the silicate fraction dominates the Li budget, followed by the oxide fraction. The least weathered leached soil (BA) has the least Li in any of the secondary fractions.

Similarly, there are no trends with depth for soil δ^7Li, except for the BA, where δ^7Li decreases linearly from 6.4 to 2.1‰ with increasing depth (Fig. 3). There is, however, a difference in the average δ^7Li_{soil} between different soil types. From least to most weathered, the V soil has an average of 1.9 ± 1.9‰, the GA of 5.2 ± 1.3‰, the BA of 2.7 ± 3.0‰, and H of -0.2 ± 3.5‰ and the HA of 0.5 ± 1.4‰. In other words, aside from the Vitrisol, the average δ^7Li_{soil} decreases as the degree of weathering increases. The parent basalt has a δ^7Li of 3.6‰, within the range for Icelandic basalts and MORB. In particular, this parent value is similar to that of 2010 Eyjafjallajökull ash (3.9‰; Pogge von Strandmann et al., 2012)), of unaltered basalt at the Reykjanes Peninsular (3.7‰; Verney-Carron et al., 2015)), and elsewhere in Iceland (3.1–4.0‰; Ryan and Kyle, 2004)), suggesting that there is little variability across Iceland, and hence of the parent composition of our different soil profiles.

4.2 Lithium in pore waters

No pore waters exist from the very fast-draining Vitrisol. In the other soils, there is a hint of increasing Li concentrations with depth in the HA and BA (Fig. 2b), but not in the other soil profiles. On average, the Li concentrations increase with increasing degree of weathering: the GA has an average pore water Li concentration of 0.09 ± 0.02 ng/ml, compared to 0.15 ± 0.07 ng/ml in the BA, 1.78 ± 1.12 ng/ml in the HA and 3.27 ± 2.54 ng/ml

in the H. In comparison, Icelandic rivers range between 0.015 and 0.4 ng/ml, although up to 1.1 ng/ml in rivers with hydrothermal input (Pogge von Strandmann et al., 2006). A Histic Andosol from elsewhere in Iceland has reported pore water Li concentrations of 0.67–1.94 ng/ml (Pogge von Strandmann et al., 2012).

There are sometimes significant differences between both the [Li] and the δ^7Li_{PW} (on average ~10‰) from the same horizons, but from the two different years/seasons, collected in September (late summer) 2009 and June (spring) 2010 (Fig. 3). Some variability between shallow (<70cm) pore waters could be expected, given fluctuations in water-levels, evaporation and redox variations, which could also explain the lack of consistent differences between the different soils. Broad patterns appear to be maintained, however; for example, in the HA, pore waters from both years trend towards lighter isotope ratios with depth (Fig. 3), similarly to broadly flat profiles in the Gleyic Andosol.

Lithium isotope ratios show trends to lower values with depth in the HA and H profiles, but not in the others. Overall, the pore water δ^7Li_{PW} is always higher than that of the soils, except at the base of the HA soil, where pore waters become similar or even slightly isotopically lighter than their corresponding soils. A precipitation correction (denoted by *) is applied to the major element pore water data, based on the assumption that rainwater in Iceland stems from the oceans (Pogge von Strandmann et al., 2006), and that all Cl^- in the pore waters stems from marine aerosols, which is validated by the low Cl^- concentrations of Icelandic basalt (Gíslason et al., 1996). We do not apply a precipitation correction to pore water Li. This is because an attempted correction using seawater elemental ratios and isotope compositions, and the measured [Cl], drives around a third of [Li] to negative values. We also note that the pore water data do not lie on a mixing trend with seawater. This is a similar approach to other basaltic Li studies (Liu et al., 2015; Pogge von Strandmann et al., 2006), and we note that this may be due to analytical uncertainty in both [Cl] and [Li] values, as also

276 suggested by other studies (Pogge von Strandmann et al., 2010). We note that for samples
277 where the correction can be made, the contribution from sea spray is generally <10%, and
278 averages <5%.

279 Between different soil profiles there are large average δ^7Li_{PW} differences that
280 correlate with the degree of weathering. The least weathered GA has the highest δ^7Li_{PW} of
281 26.7 ± 3.4‰ (1sd). The BA has an average δ^7Li_{PW} of 23.2 ± 7.3‰, the H of 14.3 ± 3.3‰ and
282 the HA of 6.6 ± 6.9‰. In comparison, Icelandic (non-hydrothermal) rivers have a δ^7Li of
283 15.4–44‰ (Pogge von Strandmann et al., 2006; Pogge von Strandmann et al., 2016; Vigier et
284 al., 2009), and another reported Icelandic Histic Andosol has pore waters that have a δ^7Li
285 ranging between 7.4–21.4‰ (Pogge von Strandmann et al., 2012).
286
287 *4.3 Lithium in secondary minerals*

288 While the fluids that correspond to the secondary minerals are not available (although
289 most were formed in the same catchment as most of the soils analysed here), analysis of the
290 solid secondary minerals, nevertheless, provides some insight into their effect on lithium
291 behaviour (Table 1). Li concentrations in the calcites are similar at 32–39 ng/g, over two
292 orders of magnitude below Icelandic basalt. Of the silicate secondary minerals, the clays have
293 Li concentrations of ~5–14 μg/g, similar to that of the Fe oxyhydroxide (14 μg/g), but
294 significantly higher than the zeolites (0.4–2.7 μg/g).

295 Li isotope ratios in the calcites range between -1.0 and 5.4‰. Inorganic calcites are
296 reported to have fractionation factors of 3–6‰ from fluid (Marriott et al., 2004). The clays
297 exhibit a similarly wide variation in δ^7Li, with values of -8.4 and 2.1‰. The zeolites tend to
298 have fairly low δ^7Li values (-4.9 to -0.2‰), except for heulandite (7.9‰) and scolecite
299 (5.3‰). Given the differing locations and the variability in the pore waters detailed above, it
300 is not possible to determine fractionation factors from these samples. As such, the Li

concentrations potentially provide more information than the isotope ratios, supporting the hypothesis that carbonate weathering does not significantly affect dissolved Li compared to silicates (Kisakürek et al., 2005). In addition, the concentration data suggest that zeolites play a more minor role in affecting Li behaviour than clays and Fe oxyhydroxides.

5.0 Discussion

5.1 Elemental depletion in soils

In Icelandic basalt weathering, Na is the most mobile major cation (Gíslason et al., 1996), consequently it goes into solution preferentially over Mg and Ca, which are approximately 10 times less mobile (Gíslason et al., 1996; Pogge von Strandmann et al., 2006). Elemental depletion in soils can be assessed from τ calculations (Brimhall and Dietrich, 1987; Chadwick et al., 1990), where the loss or gain of Li compared to the parent material is compared to that of an immobile element. Positive τ values indicate a net elemental gain, while negative ones indicate a loss. Here we use Zr as the immobile element, although we note that τ values normalised to Nb yield values within ±10%. Mobile major cations such as Mg and Ca have consistently negative τ values (aside from one sample for Mg), showing that they have been stripped from the soils. The average τ values for Mg and Ca from each soil sequence decrease with increasing weathering grade (Fig. 4a,b), agreeing with the other tracers of the degree of weathering, such as TRB. The overall τ values for these elements are higher than, for example, in the highly weathered bauxite profiles developed in the Columbia River Basalts (Liu et al., 2013), which is to be expected in the more kinetically-limited weathering regimes of Iceland (Dellinger et al., 2015).

More immobile elements, such as Al, also tend to have negative τ values in most of the samples (apart from at the base of the GA soil), albeit significantly higher numbers than the mobile elements. The Gleyic Andosol has values close to zero, and these values then

decrease with increasing grade of weathering in the other profiles (Fig. 4c). In other words, some Al has been stripped from the more weathered of these soils, but considerably less than the mobile elements, and overall elemental loss is less than in more weathered Columbia River Basalt soil profiles (where τ_{Mg} values are uniformly close to -1, and τ_{Al} values average at ~-0.55 (Liu et al., 2013)).

5.2 Soil lithium isotopes

Tau values were also calculated for Li, relative to Zr (Fig. 4d). Only the H and HA soils show any Li loss, and it is the HA that shows the greatest Li loss (average $\tau_{Li,Zr} = -0.07 \pm 0.6$), while on average the Histosol has gained Li ($\tau_{Li,Zr} = 0.19 \pm 0.7$). The BA and GA soils have gained even more Li (($\tau_{Li,Zr} = 0.27 \pm 0.15$ and 0.35 ± 0.28, respectively). The vitrisol has a tau value close to 0 (0.06), reflecting its relatively unaltered status. Positive τ values are in contrast to soil profiles from Hawaii and the Columbia River Basalts, where soils are almost always depleted in Li, and tend to exhibit much lower absolute τ_{Li} values in both settings (Liu et al., 2013; Ryu et al., 2014). Relative Li enrichment at depth in Hawaii, especially in older soils, is reported as due to Li retained in secondary minerals (Ryu et al., 2014). In the Icelandic soils examined here, the average τ_{Li} for each profile decreases with increasing weathering grade (based on TRB, and other tracers mentioned above), meaning that the nominally least weathered profiles are enriched in Li relative to the parental rock, while more weathered profiles are comparatively depleted in Li. The Gleyic Andosol in particular is increasingly enriched towards the base of the soil, and this mimics enrichment in Al (Fig. 4c), confirming that Li is being retained by secondary minerals – in this case largely allophane.

There is no direct relationship between the δ^7Li_{soil} values of individual samples and their τ_{Li} values. For example, both the Histic Andosol and especially the Histosol, show

layers that are relatively isotopically heavy compared to the rest of the soils (Fig. 3). In both cases these correspond to ash layers. In the HA profile, the ash layer is mixed with a redox layer of organic-rich material, while in the H profile it is pure ash.

Discounting those layers, however, there is a clear decrease in average δ^7Li_{soil} with increasing level of weathering, except for the Vitrisol ($\delta^7Li = 1.9 \pm 1.9‰$), which overlaps the composition of the parent basalt (3.6‰). Thus, δ^7Li values decrease from GA > BA > H ~ HA, which also broadly co-varies with the TRB values, although there is scatter within each soil type. This also yields a positive co-variation between the average τ_{Li} and the $\Delta^7Li_{soil\text{-}basalt}$ (i.e. the difference in δ^7Li between the soil and the parent basalt) for each soil type (Fig. 5). This trend is enhanced by highly depleted and isotopically light bauxites from the Columbia River Basalts (Liu et al., 2013). Various Hawaiian soils also lie on this trend (Li et al., 2020; Ryu et al., 2014), albeit with the humid profile from Li et al. (2020) having a large variability (Fig. 5).

Isotopically lighter Li isotope ratios in soils could be taken to suggest a greater Li accumulation in secondary minerals, relative to soils with heavier values (Clergue et al., 2015; Pogge von Strandmann et al., 2012). However, in the case of these soils, those that are enriched in Li relative to the parent basalt (positive τ_{Li}) are isotopically heavier compared to those that are depleted in Li. There is also an overall positive co-variation between soil δ^7Li and the abundance of clays such as allophane (Fig. 6a), which is the dominant secondary Al-silicate in these environments (Opfergelt et al., 2014; Stefansson and Gislason, 2001; Wada et al., 1992). There is no co-variation between δ^7Li_{soil} and the abundance of ferrihydrite nor clay-sized contents (Fig. 6b), showing that in these environments, Li sorption on iron oxyhydroxides or incorporation into crystalline clays is not controlling isotope fractionation. There is also is no correlation between soil δ^7Li and $\delta^{66}Zn$, where Zn is thought to be controlled by the soil organic matter content (Opfergelt et al., 2017a), suggesting that Li

376 isotopes are not affected by organic matter, as also confirmed by other studies (Li et al.,
377 2020).

378 It therefore appears that the amount of total clay-sized material in the soils is not the
379 primary control on bulk soil δ^7Li values. The correlation between δ^7Li_{soil} and allophane
380 contents (and also δ^7Li_{soil} and τ_{Li}) is also hard to understand, because soil δ^7Li values extend
381 to values both higher and lower than those of unaltered basalt, or indeed Icelandic volcanic
382 ash (Pogge von Strandmann et al., 2012). Thus, it is unlikely that the isotopically light bulk
383 soils values of the H and HA are due to a low allophane content. Instead, as discussed below
384 (Section 5.3), it appears more likely that greater allophane content is associated with higher
385 δ^7Li values because the secondary minerals are precipitating from isotopically heavy soil
386 pore waters. In other words, greater clay formation is driving pore water δ^7Li higher, from
387 which secondary minerals are then precipitating. This can occur in a standard coupled
388 relationship of two reservoirs with a constant fractionation factor (Faure, 1986). It would,
389 however, also mean that the initial dissolution of basalt would at first yield secondary
390 minerals that are isotopically lighter than basalt. This initial isotopically lightest phase is not
391 being resolved here, however. Complete loss of this phase via erosion is relatively unlikely, if
392 this phase is an aluminosilicate, because allophane is the first of these phases to form
393 (Arnalds, 2004). Therefore, such a light phase would have to be of another composition, or,
394 more likely, is not resolvable in the analysis of bulk soils due to mass balance considerations.
395 This is discussed further below in the context of the pore waters.

396 An alternate hypothesis is that the least weathered soils (BA and GA) have a higher
397 δ^7Li because they have experienced a lower solid to solution partitioning of Li, i.e. a lower
398 weathering intensity. This can be tested by comparing the measured τ_{Li} value to those based
399 on a steady-state mass balance between the dissolved load, soil and bedrock. If modelled
400 (steady-state) τ_{Li} values are similar to measured values, it would imply that the system is in

steady-state, and weathering intensity (the Li in the water/solid ratio) is controlling the soil Li gain or loss. In contrast, if modelled and measured values are not similar, then there is a decoupling between the present-day solution and solids, and more rapidly forming secondary minerals (i.e. allophane) are controlling solution compositions. We model τ_{Li} using equations from Bouchez et al., 2013:

$$w = \frac{\delta_{soil} - \delta_{rock}}{\delta_{soil} - \delta_{diss}} = -\tau^{steady-state}$$

Where δ is the δ^7Li values of the soil, rock and dissolved load. Overall, there is no relationship between the measured and modelled steady-state τ_{Li} values ($r^2 = 0.15$). However, there is a positive co-variation for the HA soils (Fig. 7), while there is none for the other soil types. This strongly suggests that the isotopically heavy soils (BA and GA) are not at steady-state between their solutions and soils, whereas the HA soil may be. In turn, this suggests that our previous hypothesis is correct, and the BA and GA soils exhibit decoupling between their solutions and soils, and therefore their high δ^7Li may be due to allophane taking up Li from heavy pore waters.

5.3 Allophane control on pore water profiles

These soils also exhibit a positive co-variation between δ^7Li_{PW} and allophane contents (significant $p<0.01$ for Spearman Rank correlation; Fig. 8). Thus, while the total clay-sized content co-varies negatively with δ^7Li_{PW} (greater clay-sized content in the poorly-drained soils), the allophane content co-varies positively with δ^7Li_{PW} (greater allophane in the rapidly-drained soils). This correlation is highly unlikely to be caused by redissolution of isotopically light clay minerals, as observed in supply-limited regimes such as the tropics (Dellinger et al., 2015), because weathering regimes in Iceland are dominantly kinetically-limited (Dellinger et al., 2015; Gíslason et al., 1996). Instead, allophane is poorly crystalline

425 and can form rapidly in these soils, and together with ferrihydrite (which does not show a
426 useful correlation with δ^7Li), tends to dominate both the secondary weathering products and
427 the exchangeable components in these volcanic soils (i.e., in many Icelandic soils it is the
428 dominant silicate secondary mineral), especially at pH > 4.9 (Opfergelt et al., 2014;
429 Sigfússon et al., 2008). As mentioned above, the similar trend in δ^7Li_{soil} with allophane
430 contents is then likely caused by allophane precipitating from isotopically heavy pore waters.
431 Formation from the congruent dissolution of volcanic ash is unlikely, because measured ash
432 has a δ^7Li lower than that of the heaviest soils (Pogge von Strandmann et al., 2012). This
433 requires that allophane precipitating from the very first step of dissolution (when solution
434 δ^7Li would presumably be close to primary rock δ^7Li) is not resolved in this study – either
435 because it is not present (unlikely, given that allophane is the first silicate secondary mineral
436 to form in Iceland (Arnalds, 2004)), or more likely that it is not resolvable in bulk soils due to
437 mass balance. A mass balance, using the fractionation factor determined below and a basaltic
438 starting composition, suggests that the first 20% of Li transferred from solution to secondary
439 minerals would have a δ^7Li <0‰, and the total δ^7Li of the solid after taking up 60% of Li
440 from solution would be +1‰. The calculations below (Section 5.4) show that, on average, 80
441 ± 27% of Li is removed from solution, which would yield a clay δ^7Li of 2.5‰, if starting
442 from congruent basaltic dissolution. In other words, the initial light precipitated solid is not
443 detectable in bulk measurements.
444 It therefore appears likely that the Li isotope composition of the pore waters is
445 largely being controlled by the formation of the more rapidly forming poorly crystalline
446 allophane, rather than the slower formation of crystalline clays such as smectite or kaolinite,
447 which are only detectable in the HA soil by XRD (Opfergelt et al., 2014). The clay fraction is
448 comprised of the <2μm fraction, so includes Fe-oxyhydroxides as well as clays. However,
449 there is no co-variation between pore water δ^7Li and Fe extracted by dithionite-citrate-

450 bicarbonate (DCB) (Opfergelt et al., 2017b), suggesting that neither crystalline clays nor Fe-
451 oxyhydroxides are controlling Li isotopes here.
452 The relatively low pH of the poorly-drained H and HA pore waters also results in a
453 co-variation between δ^7Li_{PW} and pH (Fig. 8d). Primary silicate dissolution will consume
454 protons, raising pH. In contrast, secondary mineral formation will tend to release protons,
455 thus lowering pH. Organic matter decomposition will also have the same effect (Gislason and
456 Eugster, 1987; Pogge von Strandmann et al., 2010), and in the peaty H and HA soils, it is
457 likely this latter process that is affecting pH. Thus, the soils with the highest clay-sized
458 contents have the lowest pore water pH, but this does not appear to be affecting the pore
459 water Li isotope ratio. Instead, the relationship is due to a positive co-variation between pH
460 and the saturation index of allophane. This agrees with the overall observation that allophane
461 only forms above pH 4.9 when Al stops forming a complex with humus (Mizota and van
462 Reeuwiik, 1989). This then provides further evidence that it is the formation of allophane
463 over other clays that is dominating Li isotope fractionation.
464
465 5.3.1 Using Li/Na ratios to constrain Li isotope fractionation factors
466 To further understand the processes controlling δ^7Li_{PW}, the isotope ratios can be
467 compared to the Li/Na ratios (Liu et al., 2015). In these pore waters, there is a strong negative
468 correlation between δ^7Li_{PW} and Li/Na* (Fig. 9), as would be expected if secondary minerals
469 take up Li over Na, and the lighter Li isotope preferentially. Similar relationships have been
470 seen in basaltic rivers from Iceland and elsewhere (Liu et al., 2015; Pogge von Strandmann et
471 al., 2010; Pogge von Strandmann et al., 2006; Pogge von Strandmann et al., 2016; Pogge von
472 Strandmann et al., 2017b; Vigier et al., 2009). The interesting feature concerning the
473 relationship observed here, however, is that the pore waters from the soils that have
474 undergone the most weathering (HA and H, as determined from CRB depletion) are the least

475 fractionated from basalt or bulk soils for both Li/Na and δ^7Li_{PW} (i.e. most congruent
476 dissolution), while those that have undergone the least weathering (BA and GA), and overall
477 have the lowest total clay-sized contents, are the most fractionated, implying that they also
478 have the most secondary mineral formation. In general, H and HA soils are more poorly
479 drained that BA or GA soils. In principle, that should lead to greater water-rock contact times
480 in the H and HA soils, which would promote secondary mineral formation and raise solution
481 δ^7Li (Dellinger et al., 2015; Pogge von Strandmann et al., 2017b; Pogge von Strandmann and
482 Henderson, 2015). Given that this is the opposite to what is observed, other processes must be
483 controlling the pore water δ^7Li composition.
484 Interestingly, both HA soil profiles (i.e., from this study and from Pogge von
485 Strandmann et al., 2012) plot along the same δ^7Li_{PW} vs. Li/Na trend (Fig. 9), suggesting that
486 while their isotope ratios are different, the fractionation factors are the same in both soils. In
487 other words, a different amount of Li has been removed from the water by secondary mineral
488 formation, but with the same fractionation factor. Hence, the pore waters imply that the Histic
489 Andosol from this study is dissolving almost congruently at the base of its profile (Fig. 9).
490 These are the O layers of the soil, and it may be that organic acids are driving the pH low,
491 and causing more congruent dissolution of primary and/or secondary minerals.
492 If allophane is dominating Li removal from the remaining pore waters, then it is
493 possible to calculate an isotopic fractionation factor, based on the removal of Li relative to Na
494 from solution. The logarithmic relationship between Li/Na and δ^7Li for the trend shown by
495 the GA, BA and HA pore waters can be modelled using a Rayleigh fractionation relationship.
496 The starting composition can either be set to the host soils (as in Fig. 9b), or the pristine
497 basalt. The two starting compositions make little overall difference to the fractionation factor
498 α, which varies by 0.01 according to the initial material. The average Rayleigh α value for
499 these soils is 0.993 ± 0.03 (Fig. 9b), identical to the average α value of 0.992 for all basaltic

500 rivers (Pogge von Strandmann et al., 2017b), and to the α value of 0.991 determined in
501 inorganic basalt-water weathering experiments (Pogge von Strandmann et al., 2019a).
502 Equilibrium fractionation factors are also shown in Figure 9b, but the trends of the data do
503 not appear to follow linear trends, except potentially for the HA pore waters. In general,
504 therefore, the similarity in fractionation factors between soils, inorganic experiments and
505 rivers argues that the overall fractionation of Li isotopes during basalt weathering is similar
506 regardless of first order controls, such as runoff or climate. These factors may however be the
507 cause of the scatter observed in global basaltic rivers. In addition, the similarly of the soil and
508 river fractionation factors with inorganic experiments suggests that vegetation does not form
509 a significant control on the Li isotope composition of surface waters, or that vegetation
510 imposes an identical fractionation factor.
511 In general, if most of the pore waters can be modelled by a similar fractionation
512 factor, it would supply strong evidence that one secondary mineral is dominantly removing Li
513 from solution (Hindshaw et al., 2019). In this case, given the co-variation with δ^7Li_{PW}, this
514 mineral would appear to be allophane, which also agrees with the similar values of the histic
515 andosol reported in Pogge von Strandmann et al. (2012), where allophane was also the
516 dominant silicate secondary mineral. The similar positive co-variation between bulk soil δ^7Li
517 and allophane contents could therefore also imply that the allophane is forming through
518 uptake of Li from the pore waters, driving the bulk soil Li isotope ratio heavy as well. In
519 effect, this could explain why the 'closed-system' relationship of Rayleigh fractionation
520 appears to fit the fractionation behaviour better than equilibrium fractionation. This would be
521 because allophane formation (or at least its uptake of Li) is faster than the residence time of
522 the pore waters, meaning that they behave as a closed system. This applies even to the
523 rapidly-draining BA and GA soils, suggesting that Li uptake is very rapid, and indeed water-

basalt interaction experiments show that solution δ^7Li shows more than 12‰ fractionation within 12 days, and more than 16‰ in a month (Pogge von Strandmann et al., 2019a).

5.4 Element mobility and co-variation with Li isotopes

The use of Li isotopes as a palaeo-weathering tracer (Hathorne and James, 2006; Pogge von Strandmann et al., 2017a) opens the discussion as to whether Li isotopes only inform on weathering regime changes (Dellinger et al., 2015), or whether they can inform on CO_2 drawdown efficiency (Pogge von Strandmann and Henderson, 2015). The latter requires that Li isotopes can be used to determine behaviour of the critical elements to the carbon cycle, calcium and magnesium. This can be examined through the mobility of elements, which is the tendency of elements to stay in solution (= mobile) compared to that of going into secondary minerals (=immobile) (Gíslason et al., 1996). This is determined by the ratio of the elements in question (here, Li to Ca) of the dissolved load to that of a starting composition (here, either parent basalt, or host soil). A relative mobility value of 1 implies that the Li/Ca ratio of the water is the same as that of the starting material, while lower values mean that Ca is more mobile than Li.

Icelandic rivers exhibit a very strong relationship between Li to Ca relative mobility and their δ^7Li value ($r^2 = 0.7$; Fig. 10a), as well as a similar one for Li to Mg mobility ($r^2 = 0.67$; Fig. 10c) (Pogge von Strandmann et al., 2016; Pogge von Strandmann et al., 2020). In turn, this means that Li isotopes ratios could inform on the sequestration efficiency of CO_2. The soil pore waters exhibit a similar, albeit more scattered, relationship. The GA waters have the lowest Li mobility (compared to Ca or Mg), and, given that the decrease in Li mobility is due to uptake by secondary minerals, the highest δ^7Li_{PW}. The HA and H waters show contrasting behaviour (Fig. 10a), with the HA waters having low δ^7Li_{PW} but still higher

548 Ca or Mg than Li mobility, while the H waters have intermediate δ^7Li_{PW}, but a greater Li
549 mobility than Ca.

550 When comparing the mobility vs. δ^7Li_{PW} trend of these pore waters to basaltic rivers
551 from Iceland (Pogge von Strandmann et al., 2006) and the Azores (Pogge von Strandmann et
552 al., 2010), as well as the other Icelandic Histic Andosol (Pogge von Strandmann et al., 2012),
553 the HA soils from this study lie off the overall trend. If they are removed from the overall
554 pore water trend, then that trend and its r^2 becomes similar to that for the rivers ($r^2 = 0.7$ for
555 Ca, Fig. 10a; $r^2 = 0.55$ for Mg, Fig. 10c).

556 The behaviour of the pore waters can be taken further: a simple Rayleigh relationship,
557 using the best-fit alpha value from Section 5.3.1, can be used to determine the fraction of Li
558 taken into solution (Pogge von Strandmann et al., 2012; Vigier et al., 2009)(Fig. 10b). Thus,
559 on average the GA pore waters have the lowest fraction of Li in solution (average 7 ± 4%,
560 where the uncertainty stems from the uncertainty in α), which increases to averages of 9 ±
561 6% in the BA pore waters, 14 ± 7% in the H and 50 ± 6% in the HA (up to 97% in some HA
562 waters). Again, as above, excepting the HA pore waters, there is a significant ($p<0.01$,
563 Spearman Rank) relationship between the Li to Ca relative mobility (and Li to Mg relative
564 mobility) and δ^7Li_{PW}, or the fraction of Li in solution that is derived from the δ^7Li_{PW} value
565 (Fig. 10b and d). In effect, when ~10% total Li is in solution, then Li and Ca or Mg are
566 similarly mobile (relative mobility $\sim 1^{+1.5}_{-0.5}$). In contrast, where ~2% of total Li is in solution,
567 Li is approximately a factor of 50 times less mobile than Ca (relative mobility $\sim 0.02^{+0.06}_{-0.015}$),
568 due to uptake into secondary minerals. This type of relationship has been reported in
569 experimental basalt-water interactions (Pogge von Strandmann et al., 2019a), as well as in
570 basaltic, andesitic and gneissic rivers (Clergue et al., 2015; Pogge von Strandmann et al.,
571 2010; Pogge von Strandmann et al., 2006; Pogge von Strandmann et al., 2020; Wimpenny et
572 al., 2010), and suggests that the δ^7Li value can be used to both determine the fraction of Li in

573 solution (i.e. the weathering regime) and from that the behaviour of Ca in solution. This
574 would be interesting especially from a palaeo-weathering perspective (Misra and Froelich,
575 2012; Pogge von Strandmann et al., 2017a; Pogge von Strandmann et al., 2013), because it
576 implies that the behaviour of an element directly involved in sequestering CO_2 could be
577 quantified. However, the HA pore waters here exhibit a trend with a significantly different
578 gradient from the other samples (Fig. 10b and d), and this highlights that more characterising
579 work is necessary. In this case, as mentioned above, the HA pore waters appear to follow a
580 linear rather than log trend in δ^7Li vs. Li/Na space (Fig. 9), potentially suggesting equilibrium
581 fractionation, and hence a subtly different fractionation factor. This may be because there are
582 hints that other clays are forming in these soils, compared to the other profiles (Opfergelt et
583 al., 2014; Opfergelt et al., 2017a; Opfergelt et al., 2017b).
584
585 *5.5 Li vs. Mg isotopes*
586 Magnesium is a critical element in the carbon cycle, because of the formation of Mg-
587 carbonates that sequester CO_2, and the exchange of Mg for Ca at mid-ocean ridges
588 (Humphris and Thompson, 1978; Walker et al., 1981). Mg isotopes have been suggested as a
589 tracer of Mg behaviour, but the processes that control Mg isotopes are complex, and include
590 lithology, secondary minerals and plants (Hindshaw et al., 2020; Tipper et al., 2006a; Tipper
591 et al., 2006b). It may be possible to constrain weathering processes using a combination of
592 isotopic systems, including those of Li and Mg. In particular, because Li substitutes for Mg in
593 both primary and secondary silicates (Hindshaw et al., 2019). Magnesium isotopes from these
594 particular soils and pore waters have been interpreted as representing a combination of Mg
595 adsorption by the soil exchangeable fraction (of heavy Mg isotopes preferentially) and of Mg
596 uptake by vegetation (which also takes up heavy Mg isotopes preferentially) (Opfergelt et al.,
597 2014). A strong control on Mg isotopes by adsorption onto allophane has also been reported

598 in other Icelandic soils (Pogge von Strandmann et al., 2012). When plotted against Li
599 isotopes (Fig. 11a), the pore waters are always isotopically lighter than the host basalt and
600 soils for Mg isotopes, but (as mentioned above), some pore waters have similar isotope ratios
601 to their host soils for Li isotopes.

602 Excluding the largely unfractionated HA from this study (bearing in mind that the
603 Histic Andosol studied by Pogge von Strandmann et al. (2012) behaves slightly differently –
604 Fig. 11a), there is a general negative relationship between Li and Mg isotopes, largely due to
605 the preferential uptake and sorption of light Li and heavy Mg by secondary minerals. Hence,
606 although there is scatter in any potential relationship, it is interesting that the pore waters
607 from soils that are nominally the least weathered are the most fractionated for both Li and Mg
608 isotopes. This supports the hypothesis that the secondary mineral that is affecting the sampled
609 pore waters (or at least their Li and Mg behaviour) is allophane, rather than other clays that
610 take longer to form, because it is the most fractionated (least weathered) soils that yield the
611 most favourable chemical conditions for allophane formation.

612 However, it is also clear that there is significant scatter in the relationship for these
613 pore waters between Li and Mg isotopes (Fig. 11a). In the absence of Mg-rich secondary
614 minerals in these soils (Opfergelt et al., 2014; Pogge von Strandmann et al., 2012; Sigfússon
615 et al., 2006, 2008), both Li and Mg are controlled by incorporation by substitution and
616 adsorption. However, the substitution and especially the sorption kinetics are different for the
617 two elements (experimentally by a factor of ~2.6 (Pogge von Strandmann et al., 2021b)),
618 meaning that similar behaviour will decouple the two elements and their isotopes. Scatter is
619 also caused by Mg uptake by plants, which causes isotope fractionation, and in these soils is
620 thought to be an important controlling process for Mg isotope ratios (Opfergelt et al., 2014).
621 Thus, even in the relatively simple weathering environment of Iceland, elements and isotopic

systems that are coupled by the same overall process (silicate weathering) and decoupled by the specifics of the process for each element.

5.6 Li vs. Si isotopes

Silicon is another critical element in the carbon cycle, largely because it is the weathering of silicates that ultimately removes atmospheric CO_2, and also because Si can be a critical nutrient in certain ocean environments (Frings et al., 2016; Hatton et al., 2019). Si isotopes are often interpreted similarly to Li isotopes, because secondary minerals preferentially take up the light Si isotopes, driving waters isotopically heavy, and because both trace silicate weathering processes (De la Rocha et al., 2000; Georg et al., 2007). Because of this, both isotope systems exhibit a general positive covariation when comparing all global river and pore water data (Pogge von Strandmann et al., 2017b). However, some studies, including from Iceland, have shown a significant degree of scatter between Li and Si isotopes, taken to be either influenced by plants (which preferentially take up light Si isotopes, but do not fractionate Li isotopes), or due to kinetic differences if Si is dominated by neoformation, compared to faster incorporation or adsorption for Li isotopes (Georg et al., 2007; Georg et al., 2009; Opfergelt et al., 2013; Pogge von Strandmann et al., 2006; Pogge von Strandmann et al., 2019b; Pogge von Strandmann et al., 2012; Vigier et al., 2009).

In our data, all the soils are isotopically lighter than the host basalt for Si isotopes (Fig. 11b), due to the formation of secondary minerals (Opfergelt et al., 2017b). In contrast, soil δ^7Li of the present study is only occasionally lower than the value for basalt, and there is no correlation between bulk soil δ^7Li and δ^{30}Si for any of the soil profiles. Given that secondary minerals clearly do take up the light isotopes of both elements (because pore waters are isotopically heavy), this behaviour may be a function of the overall mass balance. Because Si makes up a significant portion of clays (for example, Si makes up 20 molar% of

647 forsterite, 28% of Ca-montmorillonite and 14% of allophane), but Li does not (at most 0.01%
648 of clays), the bulk soil $\delta^{30}Si$ will be measurably perturbed by clay formation, while the bulk
649 soil $\delta^{7}Li$ will largely not be.

650 In contrast, the pore waters are clearly affected by secondary mineral formation in
651 both systems, driving an overall positive co-variation between $\delta^{7}Li$ and $\delta^{30}Si$ (Fig. 11b).
652 However, this co-variation does not exist for individual soil profiles. Further, the pore waters
653 that are most fractionated for Li isotopes (GA and BA) are not for Si, where the heaviest
654 values are from the Histosol (and also the HA of Pogge von Strandmann et al., 2012). From
655 the relationship between $\delta^{7}Li$ and Li/Na discussed above (Fig. 11a), it is clear that the Li
656 isotopes in the pore waters are only being fractionated by a single process (or processes with
657 a uniform fractionation factor), which then suggests that more variable processes are
658 affecting the Si isotope ratios of the pore waters. These likely include uptake by plants, and
659 the varying (and generally slower) kinetics that can affect the uptake of a major element into
660 secondary minerals (Opfergelt et al., 2017b; Pogge von Strandmann et al., 2012).

661 The relationships between $\delta^{7}Li$ and Mg and Si isotopes indicate the differing and
662 multiple processes that control Mg and Si over those that control Li (given the virtually linear
663 relationship between $\delta^{7}Li$ and Li/Na). This therefore demonstrates the potential
664 complications that can affect major elements over trace elements with relatively simple
665 behaviour during weathering such as Li (Pogge von Strandmann et al., 2019b), and also
666 confirms the potential of Li isotopes as a weathering tracer.

667

668 <u>6.0 Conclusions</u>

669 This study has analysed Li isotope ratios from well-studied soil and pore water
670 profiles from Iceland that have experienced different amounts of chemical weathering. Pore
671 waters from the soils that have experienced least weathering, based on the total reserve in

672 bases (Gleyic Andosol and Brown Andosol) have the highest δ^7Li_{PW} values (14–34‰), and
673 these soils are also enriched in Li compared to their parent basalts. In contrast, those that are
674 more weathered (HA and H) have the lowest δ^7Li_{PW} values (-1.4–20‰), and the bulk soils
675 are depleted in Li.

676 The pore waters form a well-defined negative trend for δ^7Li as a function of Li/Na
677 ratios, suggesting that they are controlled by a process with a single fractionation factor,
678 likely the formation of allophane. Hence, a large range of solution δ^7Li (~36‰) can be
679 generated by weathering with a single fractionation factor, due to variable proportion of Li
680 uptake. The correlation between δ^7Li and uptake presents the possibility of combining
681 isotope ratio and flux into a single solution when interpreting palaeo—records. The isotopic
682 fractionation does not correspond to the amount of clay-sized material present, but to the
683 amount of clay undergoing neoformation. In other words, it is secondary minerals that are
684 currently forming, rather those that have previously formed, which control the δ^7Li of surface
685 waters. Hence, profiles that have experienced only little overall chemical weathering, but
686 have formed a relatively large amount of amorphous, rapidly-formed, secondary minerals
687 (allophane), can exhibit substantial Li isotope fractionation.

688 Most of the pore waters also plot along the same trend between δ^7Li and the relative
689 mobility of Li to Ca or Li to Mg as other Icelandic surface waters. This suggests that
690 dissolved Li isotope ratios can be used not only to inform on Li behaviour and the silicate
691 weathering regime, but also Ca behaviour. Effectively, this can then be used to determine the
692 fraction of Ca in solution vs. secondary minerals in palaeo-records, and thus CO_2 drawdown
693 efficiency. In other words, with data from more weathering lithologies, Li isotopes may be
694 useful for quantitively determining past CO_2 drawdown behaviour.
695
696

Acknowledgements

This study and PPvS were funded by ERC Consolidator grant 682760 CONTROLPASTCO2. Birkbeck, University of London is thanked for the undergraduate project of BG. We would like to thank Kristján Jónasson and the Icelandic Institute of Natural History for providing the secondary mineral samples.

Ameijeiras-Mariño, Y., Opfergelt, S., Schoonejans, J., Vanacker, V., Sonnet, P., de Jong, J.T.M. and Delmelle, P. (2017) Impact of low denudation rates on soil chemical weathering intensity: A multiproxy approach. Chem. Geol. 456, 72–84.

Arnalds, O. (2004) Volcanic soils of Iceland. Catena 56, 3-20.

Berner, R.A., Lasaga, A.C. and Garrels, R.M. (1983) The Carbonate-Silicate Geochemical Cycle and Its Effect on Atmospheric Carbon-Dioxide over the Past 100 Million Years. Am. J. Sci. 283, 641-683.

Bouchez, J., von Blanckenburg, F. and Schuessler, J.A. (2013) Modeling novel stable isotope ratios in the weathering zone. Am. J. Sci. 313.

Brimhall, G.H. and Dietrich, W.E. (1987) Constitutive mass balance relations between chemical composition, volume, density, porosity, and strain in metasomatic hydrochemical systems: results on weathering and pedogenesis. Geochim. Cosmochim. Acta 51, 567–587.

Chadwick, O.A., Brimhall, G.H. and Hendricks, D.M. (1990) From a black to a gray box – a mass balance interpretation of pedogenesis. Geomorphology 3, 369–390.

Chan, L.H., Edmond, J.M., Thompson, G. and Gillis, K. (1992) Lithium isotopic composition of submarine basalts: implications for the lithium cycle in the oceans. Earth Planet. Sci. Lett. 108, 151-160.

Clergue, C., Dellinger, M., Buss, H.L., Gaillardet, J., Benedetti, M.F. and Dessert, C. (2015) Influence of atmospheric deposits and secondary minerals on Li isotopes budget in a highly weathered catchment, Guadeloupe (Lesser Antilles). Chem. Geol. 414, 28–41.

De la Rocha, C.L., Brzezinski, M.A. and DeNiro, M.J. (2000) A first look at the distribution of the stable isotopes of silicon in natural waters. Geochim. Cosmochim. Acta 64, 2467-2477.

Dellinger, M., Gaillardet, J., Bouchez, J., Calmels, D., Louvat, P., Dosseto, A., Gorge, C., Alanoca, L. and Maurice, L. (2015) Riverine Li isotope fractionation in the Amazon River basin controlled by the weathering regimes. Geochim. Cosmochim. Acta 164, 71–93.

Delvaux, B., Herbillon, A.J. and Vielvoye, L. (1989) Characterization of a Weathering Sequenceof Soils Derived from Volcanic Ash in Cameroon. Taxonomic, Mineralogical and Agronomic Implications. Geoderma 45, 375–388.

Faure, G. (1986) Principles of Isotope Geology, 2nd ed. Wiley.

Frings, P.J., Clymans, W., Fontorbe, G., De la Rocha, C.L. and Conley, D.J. (2016) The continental Si cycle and its impact on the ocean Si isotope budget. Chem. Geol. 425, 12–36.

736 Georg, R.B., Reynolds, B.C., West, A.J., Burton, K.W. and Halliday, A.N. (2007) Silicon isotope
737 variations accompanying basalt weathering in Iceland. Earth Planet. Sci. Lett. 261, 476-490.
738 Georg, R.B., West, A.J., Basu, A.R. and Halliday, A.N. (2009) Silicon fluxes and isotope
739 composition of direct groundwater discharge into the Bay of Bengal and the effect on the
740 global ocean silicon isotope budget. Earth Planet. Sci. Lett. 283, 67-74.
741 Gíslason, S.R., Arnorsson, S. and Armannsson, H. (1996) Chemical weathering of basalt in
742 southwest Iceland: Effects of runoff, age of rocks and vegetative/glacial cover. Am. J. Sci.
743 296, 837–907.
744 Gislason, S.R. and Eugster, H.P. (1987) Meteoric water-basalt interactions. II: A field study in
745 N.E. Iceland. Geochim. Cosmochim. Acta 51, 2841–2855.
746 Gislason, S.R., Oelkers, E.H., Eiriksdottir, E.S., Kardjilov, M.I., Gisladottir, G., Sigfusson, B.,
747 Snorrason, A., Elefsen, S., Hardardottir, J., Torssander, P. and Oskarsson, N. (2009) Direct
748 evidence of the feedback between climate and weathering. Earth Planet. Sci. Lett. 277, 213-
749 222.
750 Grimm, C., Martinez, R.E., Pokrovsky, O.S., Benning, L.G. and Oelkers, E.H. (2019)
751 Enhancement of cyanobacterial growth by riverine particulate material. Chem. Geol. 525,
752 143–167.
753 Hathorne, E.C. and James, R.H. (2006) Temporal record of lithium in seawater: a tracer for
754 silicate weathering? Earth Planet. Sci. Lett. 246, 393–406.
755 Hatton, J.E., Hendry, K.R., Hawkings, J.R., Wadham, J.L., Kohler, T.J., Stibal, M., Beaton, A.D.,
756 Bagshaw, E.A. and Telling, J. (2019) Investigation of subglacial weathering under the
757 Greenland Ice Sheet using silicon isotopes. Geochim. Cosmochim. Acta 247, 191–206.
758 Hawley, S.M., Pogge von Strandmann, P.A.E., Burton, K.W., Williams, H.M. and Gislason, S.R.
759 (2017) Continental weathering and terrestrial (oxyhydr)oxide export: Comparing glacial and
760 non-glacial catchments in Iceland. Chem. Geol. 462, 55–66.
761 Henriet, C., De Jaeger, N., Dorel, M., Opfergelt, S. and Delvaux, B. (2008) The reserve of
762 weatherable primary silicates impacts the accumulation of biogenic silicon in volcanic ash
763 soils. Biogeochemistry 90, 209–223.
764 Hindshaw, R.S., Tosca, R., Gout, T.L., Farnan, I., Tosca, N.J. and Tipper, E.T. (2019)
765 Experimental constraints on Li isotope fractionation during clay formation. Geochim.
766 Cosmochim. Acta 250, 219–237.
767 Hindshaw, R.S., Tosca, R., Tosca, N.J. and Tipper, E.T. (2020) Experimental constraints on Mg
768 isotope fractionation during clay formation: Implications for the global biogeochemical cycle
769 of Mg. Earth Planet. Sci. Lett. 531, 115980.
770 Huh, Y., Chan, L.H. and Edmond, J.M. (2001) Lithium isotopes as a probe of weathering
771 processes: Orinoco River. Earth Planet. Sci. Lett. 194, 189–199.
772 Humphris, S.E. and Thompson, G. (1978) Hydrothermal Alteration of Oceanic Basalts by
773 Seawater. Geochim. Cosmochim. Acta 42, 107-125.
774 Kennedy, M.J., Löhr, S.C., Fraser, S.A. and Baruch, E.T. (2014) Direct evidence for organic
775 carbon preservation as clay-organic nanocomposites in a Devonian black shale; from
776 deposition to diagenesis. Earth Planet. Sci. Lett. 388, 59–70.
777 Kennedy, M.J. and Wagner, T. (2011) Clay mineral continental amplifier for marine carbon
778 sequestration in a greenhouse ocean. Proceedings of the National Academy of Sciences 108,
779 9776–9781.
780 Kisakürek, B., James, R.H. and Harris, N.B.W. (2005) Li and δ^7Li in Himalayan rivers: Proxies
781 for silicate weathering? Earth Planet. Sci. Lett. 237, 387–401.

Lalonde, K., Mucci, A., Ouellet, A. and Gelinas, Y. (2012) Preservation of organic matter in sediments promoted by iron. Nature 483, 198–200.
Lechler, M., Pogge von Strandmann, P.A.E., Jenkyns, H.C., Prosser, G. and Parente, M. (2015) Lithium-isotope evidence for enhanced silicate weathering during OAE 1a (Early Aptian Selli event). Earth Planet. Sci. Lett. 432, 210–222.
Lemarchand, E., Chabaux, F., Vigier, N., Millot, R. and Pierret, M.C. (2010) Lithium isotope systematics in a forested granitic catchment (Strengbach, Vosges Mountains, France). Geochim. Cosmochim. Acta 74, 4612-4628.
Li, W. and Liu, X.-M. (2020) Experimental investigation of lithium isotope fractionation during kaolinite adsorption: Implications for chemical weathering. Geochim. Cosmochim. Acta 284, 156–172.
Li, W., Liu, X.-M. and Chadwick, O.A. (2020) Lithium isotope behavior in Hawaiian regoliths: Soil-atmosphere-biosphere exchanges. Geochim. Cosmochim. Acta 285, 175–192.
Liu, X.-L., Rudnick, R.L., McDonough, W.F. and Cummings, M.L. (2013) Influence of chemical weathering on the composition of the continental crust: Insights from Li and Nd isotopes in bauxite profiles developed on Columbia River Basalts. Geochim. Cosmochim. Acta 115, 73–91.
Liu, X.-M., Wanner, C., Rudnick, R.L. and McDonough, W.F. (2015) Processes controlling δ7Li in rivers illuminated by study of streams and groundwaters draining basalts. Earth Planet. Sci. Lett. 409, 212–224.
Maher, K. (2011) The role of fluid residence time and topographic scales in determining chemical fluxes from landscapes. Earth Planet. Sci. Lett. 312, 48–58.
Marriott, C.S., Henderson, G.M., Crompton, R., Staubwasser, M. and Shaw, S. (2004) Effect of mineralogy, salinity, and temperature on Li/Ca and Li isotope composition of calcium carbonate. Chem. Geol. 212, 5–15.
Millot, R., Vigier, N. and Gaillardet, J. (2010) Behaviour of lithium and its isotopes during weathering in the Mackenzie Basin, Canada. Geochim. Cosmochim. Acta 74, 3897–3912.
Misra, S. and Froelich, P.N. (2012) Lithium Isotope History of Cenozoic Seawater: Changes in Silicate Weathering and Reverse Weathering. Science 335, 818–823.
Mizota, C. and van Reeuwiik, L.P. (1989) Clay Mineralogy and Chemistry of Soils Formed in Volcanic Material in Diverse Climatic Regions. Soil Monograph, ISRIC, Wageningen.
Opfergelt, S., Burton, K.W., Georg, R.B., West, A.J., Guicharnaud, R.A., Sigfusson, B., Siebert, C., Gislason, S.R. and Halliday, A.N. (2014) Magnesium retention on the soil exchange complex controlling Mg isotope variations in soils, soil solutions and vegetation in volcanic soils, Iceland. Geochim. Cosmochim. Acta 125, 110–130.
Opfergelt, S., Burton, K.W., Pogge von Strandmann, P.A.E., Gislason, S.R. and Halliday, A.N. (2013) Riverine silicon isotope variations in glaciated basaltic terrains: Implications for the Si delivery to the ocean over glacial–interglacial intervals. Earth Planet. Sci. Lett. 369–370, 211–219.
Opfergelt, S., Cornelis, J.T., Houben, D., Givron, C., Burton, K.W. and Mattielli, N. (2017a) The influence of weathering and soil organic matter on Zn isotopes in soils. Chem. Geol. 466, 140–148.
Opfergelt, S., Williams, H.M., Cornelis, J.T., Guicharnaud, R.A., Georg, R.B., Siebert, C., Gislason, S.R., Halliday, A.N. and Burton, K.W. (2017b) Iron and silicon isotope behaviour accompanying weathering in Icelandic soils, and the implications for iron export from peatlands. Geochim. Cosmochim. Acta 217, 273–291.

Penniston-Dorland, S., Liu, X.-M. and Rudnick, R.L. (2017) Lithium Isotope Geochemistry, Rev. Min. Geochem., pp. 165–217.
Pistiner, J.S. and Henderson, G.M. (2003) Lithium-isotope fractionation during continental weathering processes. Earth Planet. Sci. Lett. 214, 327-339.
Pogge von Strandmann, P.A.E., Burton, K.W., James, R.H., van Calsteren, P. and Gislason, S.R. (2010) Assessing the role of climate on uranium and lithium isotope behaviour in rivers draining a basaltic terrain. Chem. Geol. 270, 227–239.
Pogge von Strandmann, P.A.E., Burton, K.W., James, R.H., van Calsteren, P., Gislason, S.R. and Mokadem, F. (2006) Riverine behaviour of uranium and lithium isotopes in an actively glaciated basaltic terrain. Earth Planet. Sci. Lett. 251, 134–147.
Pogge von Strandmann, P.A.E., Burton, K.W., Opfergelt, S., Eiriksdottir, E.S., Murphy, M.J., Einarsson, A. and Gislason, S.R. (2016) The effect of hydrothermal spring weathering processes and primary productivity on lithium isotopes: Lake Myvatn, Iceland. Chem. Geol. 445, 4–13.
Pogge von Strandmann, P.A.E., Dellinger, M. and West, A.J. (2021a) Lithium Isotopes: A Tracer of Past and Present Silicate Weathering. Cambridge University Press.
Pogge von Strandmann, P.A.E., Desrochers, A., Murphy, M.J., Finlay, A.J., Selby, D. and Lenton, T.M. (2017a) Global climate stabilisation by chemical weathering during the Hirnantian glaciation. GPL 3, 230–237.
Pogge von Strandmann, P.A.E., Elliott, T., Marschall, H.R., Coath, C., Lai, Y.J., Jeffcoate, A.B. and Ionov, D.A. (2011) Variations of Li and Mg isotope ratios in bulk chondrites and mantle xenoliths. Geochim. Cosmochim. Acta 75, 5247–5268.
Pogge von Strandmann, P.A.E., Fraser, W.T., Hammond, S.J., Tarbuck, G., Wood, I.G., Oelkers, E.H. and Murphy, M.J. (2019a) Experimental determination of Li isotope behaviour during basalt weathering. Chem. Geol. 517, 34–43.
Pogge von Strandmann, P.A.E., Frings, P.J. and Murphy, M.J. (2017b) Lithium isotope behaviour during weathering in the Ganges Alluvial Plain. Geochim. Cosmochim. Acta 198, 17–31.
Pogge von Strandmann, P.A.E. and Henderson, G.M. (2015) The Li isotope response to mountain uplift. Geology 43, 67–70.
Pogge von Strandmann, P.A.E., Hendry, K.R., Hatton, J.E. and Robinson, L.F. (2019b) The Response of Magnesium, Silicon, and Calcium Isotopes to Rapidly Uplifting and Weathering Terrains: South Island, New Zealand. Frontiers in Earth Science 7.
Pogge von Strandmann, P.A.E., James, R.H., van Calsteren, P., Gíslason, S.R. and Burton, K.W. (2008) Lithium, magnesium and uranium isotope behaviour in the estuarine environment of basaltic islands. Earth Planet. Sci. Lett. 274, 462-471.
Pogge von Strandmann, P.A.E., Jenkyns, H.C. and Woodfine, R.G. (2013) Lithium isotope evidence for enhanced weathering during Oceanic Anoxic Event 2. Nature Geoscience 6, 668–672.
Pogge von Strandmann, P.A.E., Kasemann, S.A. and Wimpenny, J.B. (2020) Lithium and Lithium Isotopes in Earth's Surface Cycles. Elements 16, 253–258.
Pogge von Strandmann, P.A.E., Opfergelt, S., Lai, Y.J., Sigfusson, B., Gislason, S.R. and Burton, K.W. (2012) Lithium, magnesium and silicon isotope behaviour accompanying weathering in a basaltic soil and pore water profile in Iceland. Earth Planet. Sci. Lett. 339–340, 11–23.

873 Pogge von Strandmann, P.A.E., Renforth, P., West, A.J., Murphy, M.J., Luu, T.-H. and
874 Henderson, G.M. (2021b) The lithium and magnesium isotope signature of olivine
875 dissolution in soil experiments. Chem. Geol. 560, 120008.
876 Raymo, M.E. and Ruddiman, W.F. (1992) Tectonic Forcing of Late Cenozoic Climate. Nature
877 359, 117-122.
878 Revels, B.N., Rickli, J., Moura, C.A.V. and Vance, D. (2021) Nickel and its isotopes in the
879 Amazon Basin: The impact of the weathering regime and delivery to the oceans. Geochim.
880 Cosmochim. Acta 293, 344–364.
881 Ryan, J.G. and Kyle, P.R. (2004) Lithium abundance and lithium isotope variations in mantle
882 sources: insights from intraplate volcanic rocks from Ross Island and Marie Byrd Land
883 (Antarctica) and other oceanic islands. Chem. Geol. 212, 125–142.
884 Ryu, J.-S., Vigier, N., Lee, S.-W., Lee, K.-S. and Chadwick, O.A. (2014) Variation of lithium
885 isotope geochemistry during basalt weathering and secondary mineral transformations in
886 Hawaii. Geochim. Cosmochim. Acta 145, 103–115.
887 Sigfússon, B., Gislason, S.R. and Paton, G.I. (2006) The effect of soil solution chemistry on
888 the weathering rate of a Histic Andosol. Journal of Geochemical Exploration 88, 321-324.
889 Sigfússon, B., Gislason, S.R. and Paton, G.I. (2008) Pedogenesis and weathering rates of a
890 Histic Andosol in Iceland: Field and experimental soil solution study. Geoderma 144, 572-
891 592.
892 Stefansson, A. and Gislason, S.R. (2001) Chemical weathering of basalts, Southwest Iceland:
893 Effect of rock crystallinity and secondary minerals on chemical fluxes to the ocean. Am. J.
894 Sci. 301, 513-556.
895 Steinhoefel, G., Brantley, S.L. and Fantle, M.S. (2021) Lithium isotopic fractionation during
896 weathering and erosion of shale. Geochim. Cosmochim. Acta 295, 155–177.
897 Teng, F.Z., Li, W.Y., Rudnick, R.L. and Gardner, L.R. (2010) Contrasting lithium and
898 magnesium isotope fractionation during continental weathering. Earth Planet. Sci. Lett. 300,
899 63-71.
900 Tessier, A., Campbell, P.G.C. and Bisson, M. (1979) Sequential Extraction Procedure for the
901 Speciation of Particulate Trace Metals. Analytical Chemistry 51, 844-851.
902 Tipper, E.T., Galy, A. and Bickle, M.J. (2006a) Riverine evidence for a fractionated reservoir
903 of Ca and Mg on the continents: Implications for the oceanic Ca cycle. Earth Planet. Sci. Lett.
904 247, 267-279.
905 Tipper, E.T., Galy, A., Gaillardet, J., Bickle, M.J., Elderfield, H. and Carder, E.A. (2006b) The
906 magnesium isotope budget of the modern ocean: Constraints from riverine magnesium
907 isotope ratios. Earth Planet. Sci. Lett. 250, 241-253.
908 Verney-Carron, A., Vigier, N., Millot, R. and Hardarsson, B.S. (2015) Lithium isotopes in
909 hydrothermally altered basalts from Hengill (SW Iceland). Earth Planet. Sci. Lett. 411, 62–71.
910 Vigier, N., Decarreau, A., Millot, R., Carignan, J., Petit, S. and France-Lanord, C. (2008)
911 Quantifying Li isotope fractionation during smectite formation and implications for the Li
912 cycle. Geochim. Cosmochim. Acta 72, 780–792.
913 Vigier, N., Gislason, S.R., Burton, K.W., Millot, R. and Mokadem, F. (2009) The relationship
914 between riverine lithium isotope composition and silicate weathering rates in Iceland. Earth
915 Planet. Sci. Lett. 287, 434–441.
916 Wada, K., Arnalds, O., Kakuto, Y., Wilding, L.P. and Hallmark, C.T. (1992) Clay minerals of
917 four soils formed in eolian and tephra materials in Iceland. Geoderma 52, 351-365.

Walker, J.C.G., Hays, P.B. and Kasting, J.F. (1981) A Negative Feedback Mechanism for the Long-Term Stabilization of Earths Surface-Temperature. Journal of Geophysical Research-Oceans and Atmospheres 86, 9776-9782.
West, A.J., Galy, A. and Bickle, M. (2005) Tectonic and climatic controls on silicate weathering. Earth Planet. Sci. Lett. 235, 211–228.
Wimpenny, J., James, R.H., Burton, K.W., Gannoun, A., Mokadem, F. and Gislason, S.R. (2010) Glacial effects on weathering processes: New insights from the elemental and lithium isotopic composition of West Greenland rivers Earth Planet. Sci. Lett. 290, 427-437.

Bulk soils				C	CEC	TRB	Ferrihydrite	Allophane	Total clay	Na	Al	Fe	Ca	Mg	Zr	Li	δ^7Li	2sd
Soil name	ID	Horizon	Depth (cm)	**%**	cmolc.kg-1	cmolc.kg-1	%	%	%	g/kg	g/kg	g/kg	g/kg	g/kg	µg/g	µg/g	‰	
Histic Andosol	HA	A1	0-15	18.5	40.1	148	7.1	4.9	56.1	4.3	50.5	165.7	14.6	6.4	167	4.70	0.9	0.3
		A2	15-26	16.9	55.3	177	5.4	9.5	54.3	5.5	72	98.9	17.7	7.3	237	5.80	-0.3	0.2
		Bw1	26-40	14.5	61.8	138	11.9	8.3	55.2	4.4	60.4	175.1	13.8	5.6	201	4.60	1.4	0.3
		Bw2	40-57	16.9	53.8	156	7.1	6.9	45.5	6.5	63	164.4	16.1	5.0	263	4.53	-0.7	0.4
		O1	57-67	28.7	59.4	103	4.4	6.6	53.8	3.3	44	55.7	11	3.9	275	2.36	-0.8	0.3
		redox	67-83	12.8	28.3	332	1.4	6.9		18.7	78.6	57.6	30.2	9.9	431	11.0	3.0	0.2
		O2	83+	42.7	71.3	52.4	3.2	1.4	55.3	2.1	22.3	42.9	5.4	1.7	280	3.21	0.3	0.5
Histosol	H	O1	0-13	21.0	49.5	266	6.8	2.5	52.3	6.4	39.5	120.3	28.5	11.1	112	7.86	-1.1	0.2
		O2	13-26	22.9	39.5	192	3.8	1.8	8.4	5.6	37	83.8	19.2	8.1	131	6.30	-4.3	0.3
		O3	26-40	18.6	52.6	188	5.9	6.7	38.2	7.5	56.4	141.7	18.6	6.8	252	4.32	0.3	0.3
		T	40-52	12.0	43.2	60.9	43.5	9.8		1.2	20.9	341.5	7.6	2.1	74	0.83	6.9	0.5
		O4	52-63	10.3	30.0	283	3.3	4.6	44.4	15.1	63.4	101.6	26.4	8.6	339	10.3	-0.7	0.4
		O5	63-72	29.3	65.6	115	4.7	2.3	70.9	2.8	34.3	140.7	12.6	4.6	132	2.04	0.0	0.3
		O6	72+	30.4	85.3	118	3.9	3.5	42.7	3.6	35.5	86.6	12.7	4.4	212	4.54	-2.2	0.2
Brown Andosol	BA	A1	0-21	7.29	36.8	403	7.8	10.7	33.2	10	83.2	111.9	39.1	19.2	223	9.05	6.4	0.5
		A2	21-40	7.92	35.2	370	8.6	11.0	29.7	9.6	86.8	117.2	36.1	17.2	241	8.97	5.0	0.4
		Bw1	40-52	6.47	36.8	377	7.3	9.2	37.2	10.1	91.3	122.7	35.7	17.8	217	9.66	3.9	0.2
		Bw2	52-96	7.25	50.9	317	9.7	13.0	41.0	8.5	97	126.1	31.1	14.5	262	9.08	3.7	0.2
		Bw3/C	96+	5.71	42.7	324	8.5	12.6		9.8	94.4	127.9	31.5	14.1	246	11.8	2.1	0.4
Gleyic Andosol	GA	A1	0-12	9.51	47.0	333	7.4	9.8	37.1	7.3	84.1	104.5	30.7	17.3	191	8.94	5.6	0.3
		A2	12-29	6.20	46.5	377	8.5	12.2	41.2	7.7	85.1	119.2	35	19.7	218	10.3	5.1	0.3
		Bw1	29-43	6.86	46.7	275	6.4	14.7	38.9	7.3	91	116.7	27.5	12.2	250	10.3	6.6	0.4
		Bw2	43-56	6.76	49.9	293	4.6	15.4	36.3	7.6	93.6	105.5	29.7	12.8	262	11.0	5.0	0.3
		C	56-64	2.70	23.5	649	4.0	7.4		10.3	78.3	119.2	38	38	144	8.92	6.3	0.3
		2Bw1	64+	3.26	40.2	480	1.8	21.1	22.9	8.5	112.5	59.2	22.5	22.5	196	16.6	5.3	0.3
Vitrisol	V	A	0-9	0.32	13.2	667	3.9	8.9	4.6				61.5	32.0	235	10.8	2.1	0.5
		B/C	9-33	0.26	32.7	568	7.1	14.2	4.6				53	27.9	219	9.08	3.6	0.3
		C	33+		8.87										137	4.98	-0.2	0.1
Parental basalt										20.6	72.6	103.8	74	32.1	164	5.89	3.6	0.3
Secondary minerals																		
Calcite	Iceland spar									0.38	0.02	0.009	336	0.01				
Calcite	11551									0.30	0.03	0.003	346	3.32		0.04	0.4	0.6
Calcite	11547									0.29	0.05	0.028	358	3.77		0.03	-1.0	0.5
Calcite	7869									0.33	0.39	0.133	363	0.19		0.04	5.4	0.5
Clay	11571									0.40	83.6	292	6.10	55.7		13.4	-8.4	0.2
Clay	21637									3.38	55.2	109	11.8	16.7		5.35	2.1	0.2
Heulandite	11607									9.52	68.1	0.010	29.5	0.05		0.83	7.9	0.3
Chabazite	15227									6.07	89.7	0.12	49.5	0.07		1.00	-0.2	0.2
Mesolite	21633									29.0	139.5	1.17	72.4	0.75		2.29	-4.9	0.2
Stilbite	11933									11.9	72.1	7.60	36.8	2.88		2.09	-1.8	0.1
Epistilbite	11613									11.9	97.9	0.057	57.2	0.03		2.57	-1.0	0.3
Scolecite	4221									16.8	102	0.060	43.1	0.02		2.33	5.3	0.6
Fe-oxyhydroxide	A6									11.0	110	283	55.6	27.7		14.1		
Leaches (% Li of total)			Exchangeable		Carbonate	Oxide	Residue											
HA 01			1.4		3.2	25.6	69.9											
H O6			3.4		4.0	20.6	72.0											
BA BW2			0.2		0.9	9.8	89.1											

Table 1. Bulk soil and secondary mineral data. All soil data aside from Li isotope ratios are from Opfergelt et al., 2014. The final section shows the results for Li from sequential leaching of three soils.

Pore waters	Depth	pH	T	Li	Na	Mg	Al	K	Ca	Si	Fe	Cl	δ^7Li	2sd
	cm		°C	ng/ml	µg/ml	µg/ml	ng/ml	µg/ml	µg/ml	µg/ml	ng/ml	µg/ml	‰	
2009														
HA H1	7.5	6.18	11.6	0.61	16.5	5.19	185	5.64	5.86	8.37	40.4	34.0	15.5	0.3
HA O1	62	3.64	11	3.02	7.87	3.60	10200	0.116	30.1	31.1	115	11	2.1	0.1
HA O2	83	3.71	10.9	3.02	8.95	3.56	9670	0.127	24.4	30.8	122	12	-1.4	0.2
H O1	6.5	4.34	11.3	4.17	9.17	4.16	316	0.390	9.88	17.40	13.8	9.0	14.6	0.5
H O5	67.5	4.78	11.7	3.02	16.1	3.33	15.8	0.318	4.29	13.90	519	22	14.3	0.3
H O6	72	5.48	11.6	5.94	19.6	10.9	90.8	0.746	11.2	18.3	25000	21	10.7	0.4
BA BW1	46	5.83	11.9	0.04	7.26	0.73	90.2	0.036	1.64	0.74	65.8	14.2	34.2	0.1
GA A1	6	5.64	13.1	0.12	7.83	1.46	106	0.326	3.78	4.89	38.6	25.9	28.5	0.3
GA BW1	36	5.90	13	0.08	7.53	1.20	9.6	0.041	3.54	7.95		13.6	34.2	0.2
GA 2BW1	64	5.88	12.9	0.08	6.93	2.00	11.6	0.011	5.94	13.80		12.1	29.5	0.4
2010														
HA H1	7.5	5.05	19.6	0.61	12.6	8.64	320	3.32	11.3	9.60	26.5	7.9	12.3	0.4
HA BW1	33	4.67	20.3	0.71	8.29	3.67	475	0.089	16.2	9.60	22.8	12.1	15.1	0.3
HA 01	62	3.99	18.9	1.80	6.70	4.13	6510	0.088	27.8	24.2	32.3	10.0	7.4	0.1
HA redox	75	3.98	18.5	2.97	8.54	3.60	7530	0.128	23.2	26.5	36.2	11.3	0.8	0.2
HA O2	83	3.95	18.3	2.80	9.52	4.34	7640	0.078	24.5	30.3	36.5	13.0	0.8	0.4
H O1	6.5	4.88	22.3	2.86	9.91	4.68	54.3	3.13	7.20	10.5	282	4	19.7	0.3
H O2	19.5	5.47	20.3	0.79	12.0	6.38	23.8	0.439	7.26	5.30	58.5	28.7	18.4	0.4
H O3	33	5.15	19.2	1.95	14.7	4.53	205	0.315	8.94	17.4	193	23	11.7	0.3
H O4	57.5			3.27	21.0	6.12	101	0.788	7.14	19.2	15300		14.1	0.6
H O6	72			7.48	25.4	17.1	45.7	1.72	15.2	18.8	20000		11.3	0.4
BA A1	10.5			0.06	6.38	1.51	4.93	1.23	2.13	5.90	12.1		28.4	0.6
BA A2	30.5	5.84	19.1	0.14	5.18	0.74	3.54	0.063	1.11	3.50	9.86	9.60	18.6	0.3
BA BW1	46	5.88	19	0.25	6.89	0.93	50.8	0.043	1.55	3.60	34.5	13.5	13.7	0.3
BA BW2	74	5.96	19.1	0.14	7.22	0.74	4.61	0.040	1.52	4.40	8.03	15.50	18.4	0.4
BA BW3	96	5.46	20	0.14	8.05	0.92	1.57	0.101	1.80	5.00	3.51	14.20	20.5	0.2
GA A1	6			0.05	6.87	1.79	17.3	2.318	3.75	5.70	13.6		31.6	0.4
GA A2	20.5	5.77	17.8	0.12	6.69	0.68	28.2	0.995	1.55	7.50	45.4	6.6	24.3	0.2
GA BW2	36			0.09	6.65	0.68	5.69	0.173	1.76	8.10	14.7		27.0	0.5
GA BW2	49.5	5.6	17.4	0.10	8.28	1.27	40.0	0.280	3.75	12.0	11.3	8.5	22.1	0.2
GA 2BW1	64	5.46	17.2	0.08	11.3	2.48	10.4	0.368	7.14	12.4	4.96	9.30	25.6	0.2

Table 2. Pore water data. All data aside from Li isotope ratios are from Opfergelt et al., 2014.

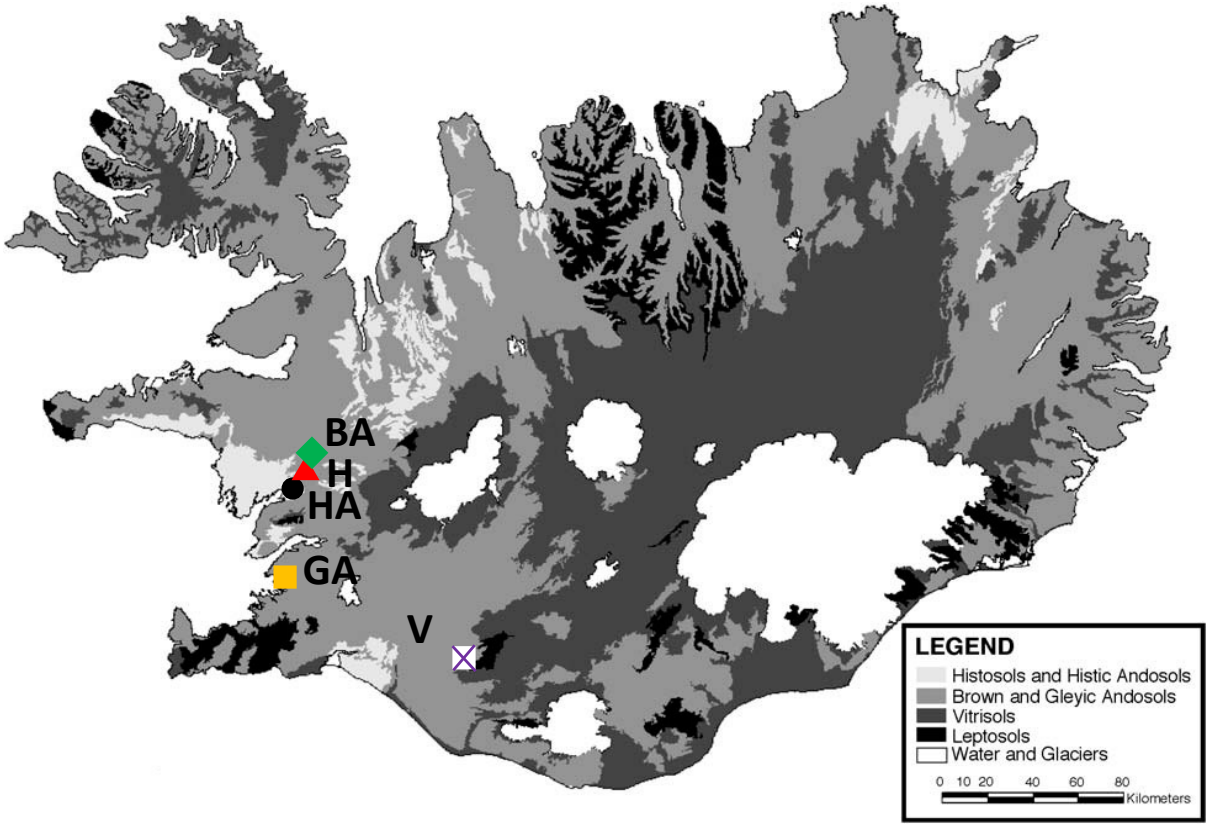

954

955 Figure 1. Sample locations on a soil map of Iceland. Soil symbols correspond to the key of

956 Figure 2. Adapted from Opfergelt et al., 2014.

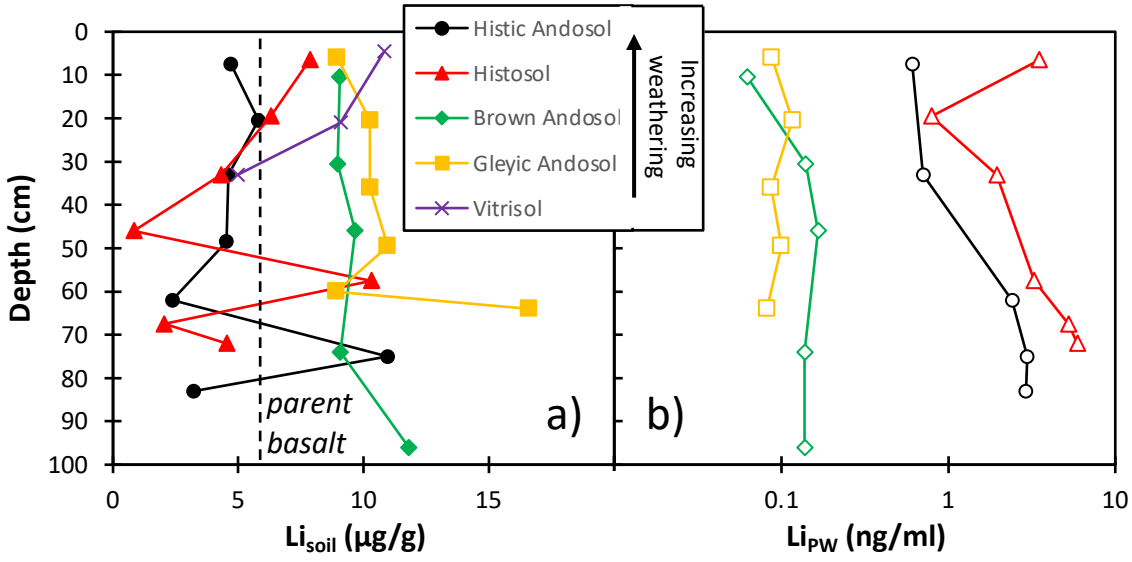

957

Figure 2. Depth profiles for Li concentrations for bulk soils and parent basalt depicted by the vertical dashed line (a), and pore waters (b). The pore water concentrations have been averaged from the two different collection years for this diagram (Table 2).

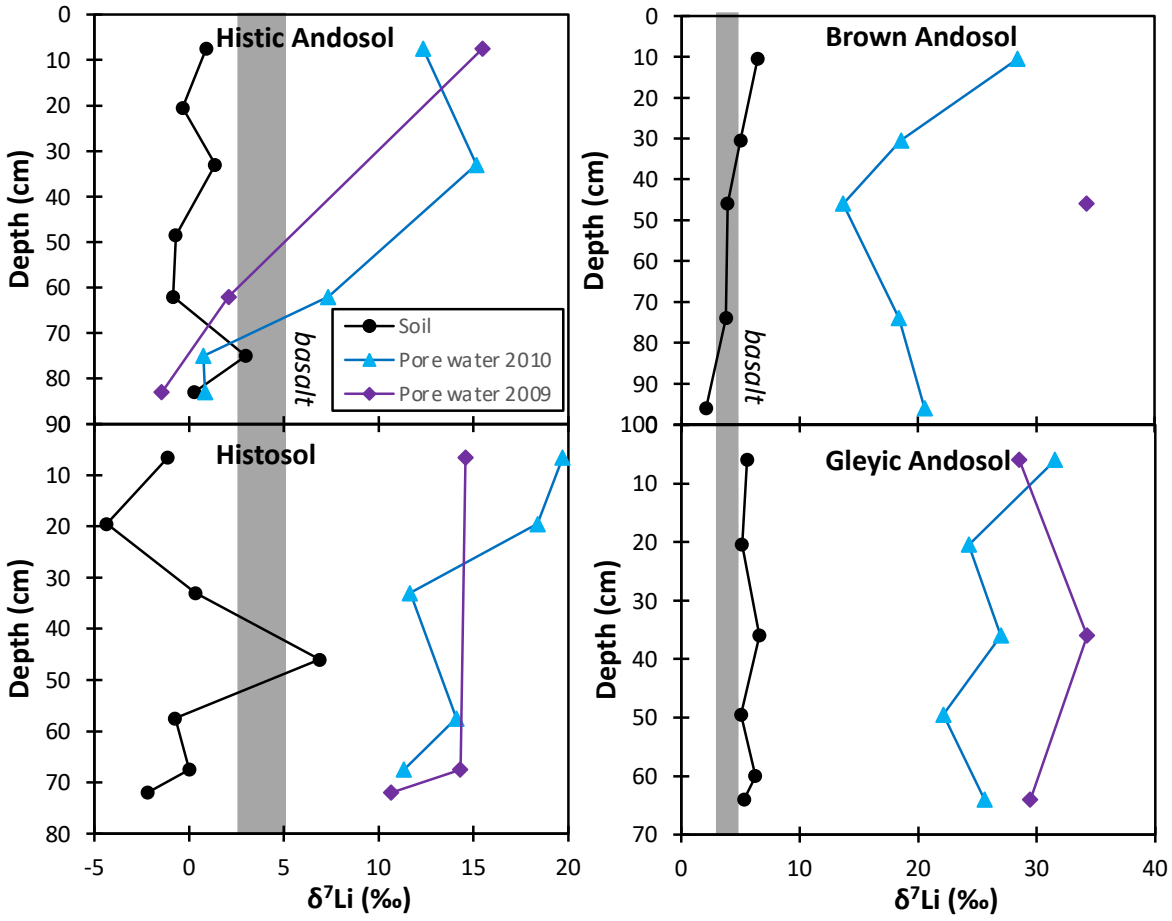

Figure 3. Li isotope depth profiles for bulk soils, and the two different seasons of pore waters. In 2009, samples were taken in September (late summer), while in June (late spring) in 2010. The range of Icelandic basalt is depicted by the shaded area. Note the difference in horizontal axis scales.

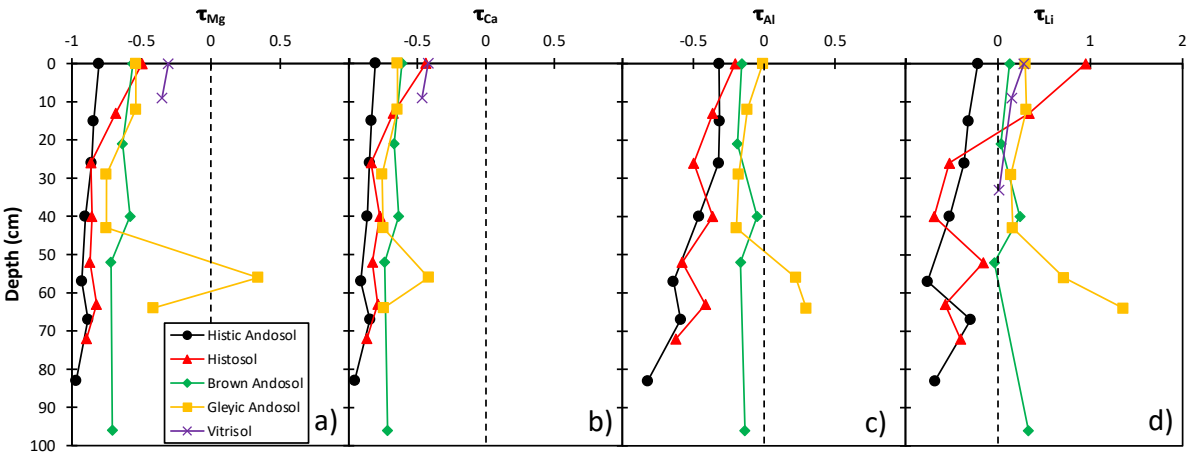

Figure 4. Tau values for the soils for the elements Mg, Ca, Al and Li. The dashed vertical lines are at tau = 0.

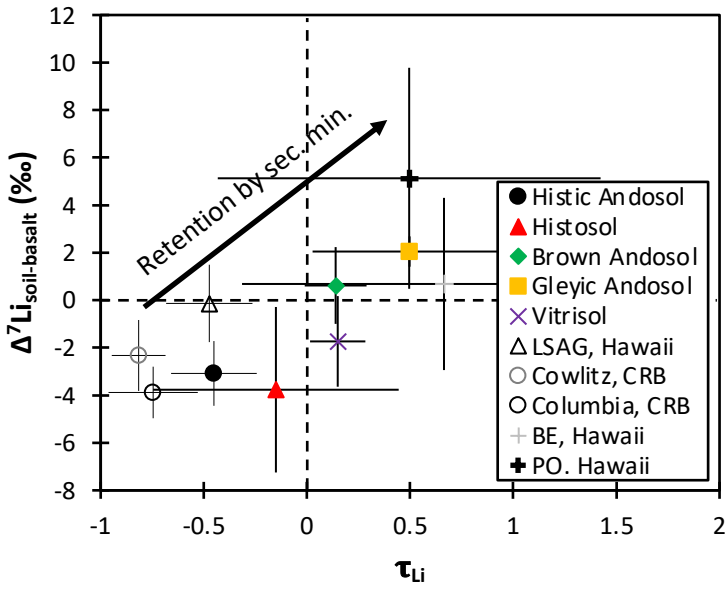

983

984 Figure 5. Average τ_{Li} and $\Delta^7Li_{soil\text{-}basalt}$ values for each soil profile. The error bars represent the

985 1sd spread in the data. Also shown are data from the Columbia River Basalts (Liu et al.,

986 2013) and multiple sections from Hawaii (Li et al., 2020; Ryu et al., 2014). Due to high

987 aeolian input, the topsoil from Li et al. (2020) has been removed from the averages.

988

989

990

991

992

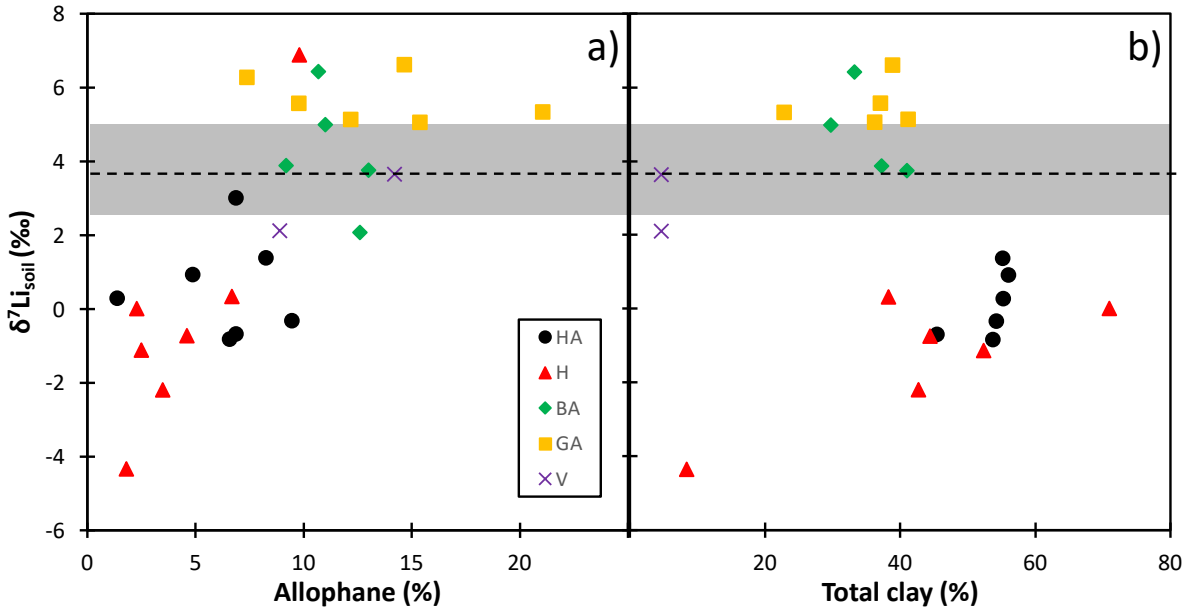

Figure 6. Bulk soil Li isotopes as a function of allophane content (a) and total clay-sized content (b).

1010

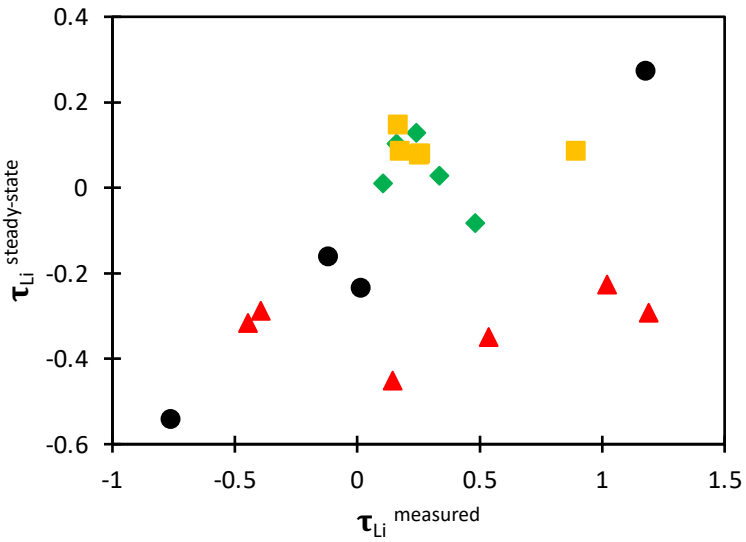

1011

1012 Figure 7. Comparison of measured τ_{Li} values, compared to steady-state τ_{Li} values calculated

1013 from Li isotope ratios (Bouchez et al., 2013). Co-variation (as for HA soils) would suggest

1014 that depletion or enrichment may be due to weathering intensity, while no correlation (as for

1015 the other soils) suggest decoupling between processes controlling soil and present-day water

1016 composition. See text for details. Symbols are the same as figure 6.

1017

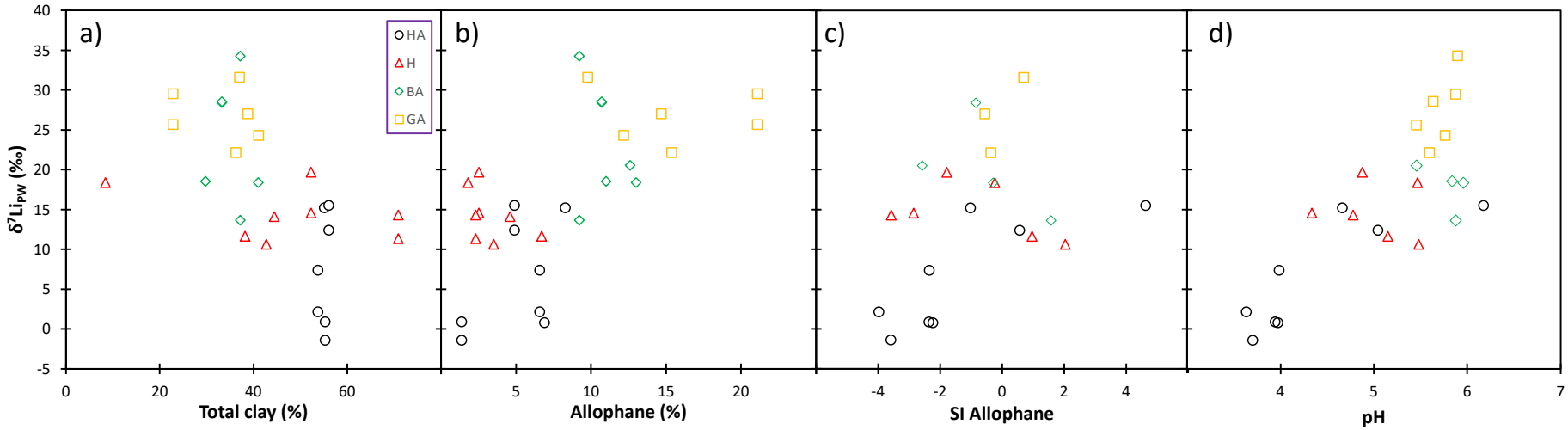

1018

1019 Figure 8. Pore water Li isotope ratios as a function of soil total clay content (a), soil allophane content (b), and the PHREEQC-derived allophane

1020 saturation index (c), and pH (d).

1021

1022

1023

1024

1025

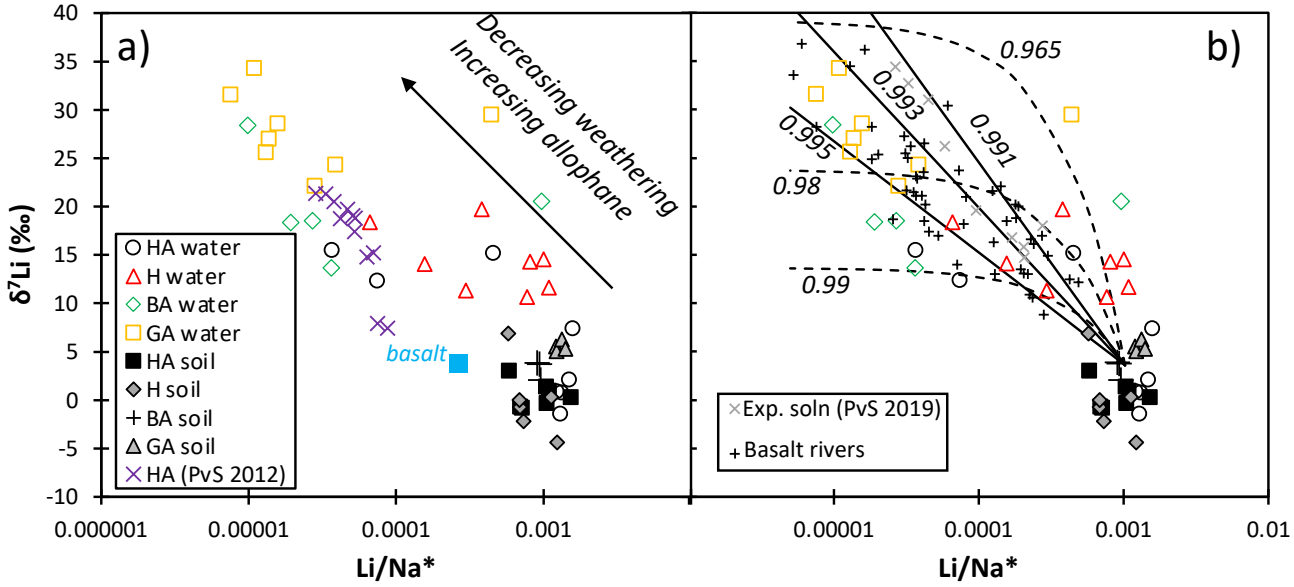

Figure 9. (a) Li isotope ratios as a function of Li/Na ratios. The pore waters from the Histic Andosol of Pogge von Strandmann et al. (2012) are also shown. (b) the same diagram as panel a, but with Rayleigh (solid lines) and equilibrium (dashed lines) fractionation paths. The numbers next to each line represent the fractionation factor α. Experimental solutions from basalt weathering experiments (Pogge von Strandmann et al., 2019a), and Icelandic rivers (Pogge von Strandmann et al., 2006) are also shown. The * in the axis titles denote precipitation-corrected values.

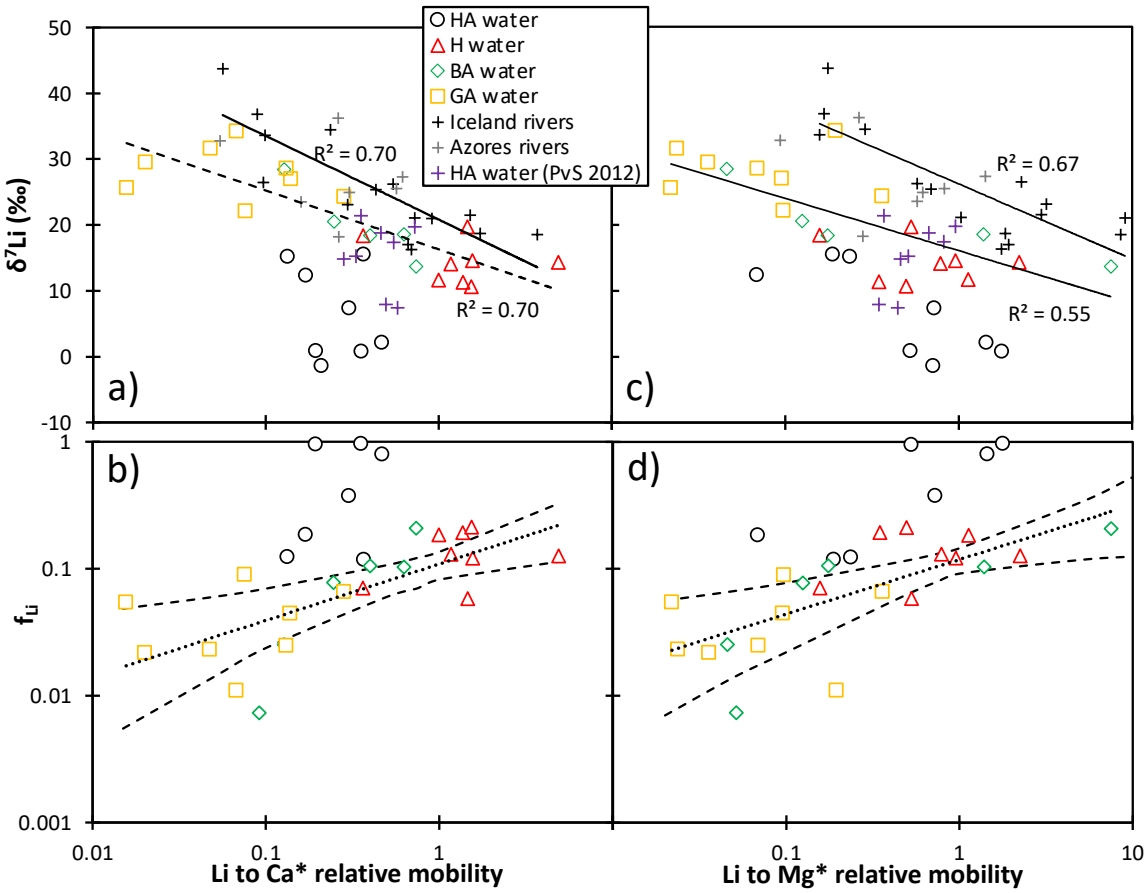

Figure 10. a) Surface water Li isotope ratios as a function of the relative mobility of Li to Ca. The dashed trend line is the fit to this study's pore waters (excluding the HA waters – see text). The solid line is the fit to Icelandic rivers (Pogge von Strandmann et al., 2006). Rivers from the Azores (Pogge von Strandmann et al., 2010) are also shown. b) the fraction of total Li in solution as a function of the Li to Ca relative mobility. The dotted line is the trend line, while the dashed lines are 95% confidence intervals. Panels c and d represent the same trends, except for the relative mobility of Li to Mg. The * in the axis titles denote precipitation-corrected values.

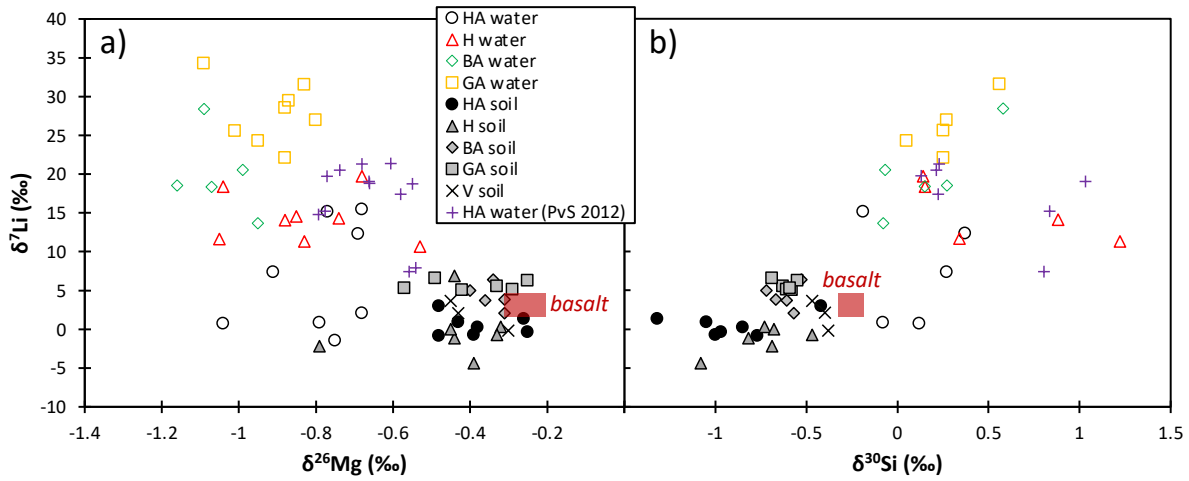

Figure 11. (a) Li isotope ratios as a function of Mg isotope ratios (Opfergelt et al., 2014; Pogge von Strandmann et al., 2012); (b) Li isotopes as a function of Si isotope ratios (Opfergelt et al., 2017b; Pogge von Strandmann et al., 2012).